BACKGROUND ELIMINATION

IN DIGITAL IN-LINE HOLOGRAMS

Phacharawadee Raweng

A Thesis Submitted in Partial Fulfillment of the Requirements for

the Degree of Master of Science in Laser Technology

Suranaree University of Technology

Academic Year 2006

การกำจัดพื้นหลังในอินไลน์ฮอโลแกรมเชิงตัวเลข

นางสาวพัชราวดี ระเวง

วิทยานิพนธ์นี้เป็นส่วนหนึ่งของการศึกษาตามหลักสูตรปริญญาวิทยาศาสตรมหาบัณฑิต
สาขาวิชาเทคโนโลยีเลเซอร์
มหาวิทยาลัยเทคโนโลยีสุรนารี
ปีการศึกษา 2549

BACKGROUND ELIMINATION

IN DIGITAL IN-LINE HOLOGRAMS

Suranaree University of Technology has approved this thesis submitted in partial fulfillment of the requirements for the Degree of Master of Science.

Thesis Examining Committee

_____

(Assoc. Prof. Dr. Prapun Manyum)

Chairperson

_____

(Assoc. Prof. Dr. Joewono Widjaja)

Member (Thesis Advisor)

_____

(Assoc. Prof. Dr. Yupeng Yan)

Member

_____

(Assoc. Prof. Dr. Saowanee Rattanaphani)

Vice Rector for Academic Affairs

_____

(Assoc. Prof. Dr. Sompong Thammathaworn)

Dean of Institute of Science

พัชราวดี ระเวง : การกำจัดพื้นหลังในอินไลน์ฮอโลแกรม (BACKGROUND ELIMINATION IN DIGITAL IN-LINE HOLOGRAMS) อาจารย์ที่ปรึกษา : รองศาสตราจารย์ ดร. ยูโวโน วิดจายา, 61 หน้า

งานวิทยานิพนธ์นี้ได้ทำการศึกษาการปรับปรุงคุณภาพของภาพรีคอนสตรัคจากอินไลน์ฮอโลแกรมด้วยการกำจัดพื้นหลังโคฮีเรนท์เอกรูปโดยวิธีจำลองสถานการณ์ด้วยคอมพิวเตอร์ โดยสร้างฮอโลแกรมของวัตถุแบบเส้นและแบบจัตุรัสทั้งจำนวนเดี่ยวและพหุคูณด้วยวิธีการเชิงเลข ซึ่งคำนวณจากปริพันธ์การเลี้ยวเบนแบบเฟรสเนล ทั้งนี้การขจัดพื้นหลังโคฮีเรนท์ทำได้จากการลบฮอโลแกรมจำลองด้วยค่าเฉลี่ยความเข้มของฮอโลแกรม ซึ่งคุณภาพของภาพรีคอนสตรัคที่ได้จากฮอโลแกรมอันได้ถูกปรับปรุงนี้สามารถวัดได้จากการคำนวณหาอัตราส่วนระหว่างสัญญาณสูงสุดต่อสัญญาณรบกวน ในกรณีของพหุคูณวัตถุได้สร้างฮอโลแกรมของวัตถุซึ่งอยู่ในระนาบเดียวกันและต่างระนาบกัน ผลที่ได้แสดงให้เห็นว่าคุณภาพของภาพรีคอนสตัคที่ได้จากฮอโลแกรมซึ่งไม่มีพื้นหลังโคฮีเรนท์นั้นดีกว่าผลที่ได้จากฮอโลแกรมต้นแบบทั้งวัตถุแบบเส้นและแบบจัตุรัส ส่วนในกรณีฮอโลแกรมของพหุคูณวัตถุนั้นก็ได้ผลเช่นเดียวกัน อย่างไรก็ตามคุณภาพของภาพรีคอนสตรัคที่ได้จะลดลงเมื่อจำนวนและขนาดของวัตถุเพิ่มขึ้น

สาขาวิชาเทคโนโลยีเลเซอร์และโฟตอนนิกส์ ลายมือชื่อนักศึกษา _____

ปีการศึกษา 2549 ลายมือชื่ออาจารย์ที่ปรึกษา _____

PHACHARAWADEE RAWENG : BACKGROUND ELIMINATION IN DIGITAL IN-LINE HOLOGRAMS. THESIS ADVISOR : ASSOC. PROF. JOEWONO WIDJAJA, Ph.D. 61 PP.

COHERENT BACKGROUND REMOVAL/TWIN IMAGE PROLEM/IN-LINE HOLOGRAPHY

Quality improvement of reconstructed images from in-line holograms by eliminating a uniform coherent background is studied through computer simulations. Single and multiple line and square objects are used as specimens of the holograms which are numerically generated by using a Fresnel diffraction integral. The coherent background is removed by subtracting the simulated hologram with its averaging intensity. The quality of the image reconstructed from this modified hologram is measured by calculating a peak signal to noise ratio (PSNR). In the case of the multiple objects, the holograms of objects distributed in-plane and out-of-plane are generated. The results show that the quality of images reconstructed from the holograms without the coherent background is higher than that of the original hologram for both line and square objects. As for the case of the holograms of multiple objects, the similar result is also obtained. However, the quality reduces as the number and the size of the object become larger.

School of Laser Technology and Photonics Student's Signature _____

Academic Year 2006 Advisor's Signature _____

ACKNOWLEDGEMENTS

I would like to express my gratitude to Assoc. Prof. Dr. Joewono Widjaja for his continuous guidance, help and encouragement throughout the course of this study. I am indebted to his valuable insights and constructive comments on my work. This thesis would not have reached completion without his constant encouragement and support.

I wish to express my special thank to Dr. Siriwat Soontaranon for his technical assistance throughout my research study.

Finally, I am indebted to my family for their love and encouragement throughout my studies.

Phacharawadee Raweng

CONTENTS

Page

ABSTRACT IN THAI I

ABSTRACT IN ENGLISH II

ACKNOWLEDGEMENTS III

CONTENTS IV

LIST OF TABLES VII

LIST OF FIGURES VII

CHAPTER

I INTRODUCTION 1

1.1 Background 1

1.2 Significant of the study 3

1.3 Research objective 3

1.4 Scope and limitation of the study 3

1.5 Organization 4

II IN-LINE HOLOGRAPHY 5

2.1 Hologram formation 5

2.1.1 Hologram of multiple-objects 6

2.1.1.1 In-line hologram of multiple-line object 8

2.1.1.2 In-line hologram of multiple-square object 15

2.2 Image reconstruction 20

CONTENTS (Continued)

Page

III IMAGE RECONSTRUCTIONS FROM IN-LINE HOLOGRAM OF SINGLE OBJECT 28

3.1 Removal of virtual image and uniform background from holograms 28

IV IMAGE RECONSTRUCTIONS FROM IN-LINE HOLOGRAM OF MULTIPLE OBJECTS 38

4.1 Image reconstructions from in-line holograms of in-plane objects 38

4.2 Image reconstructions from in-line holograms of out-of-plane objects 46

VII CONCLUSIONS 55

REFERENCES 58

CURRICULUM VITAE 61

LIST OF FIGURES

Figure **Page**

2.1 Optical system for recording an in-line (Gabor) hologram. 5

2.2 Schematic diagram of setup for recording hologram of three objects. 7

2.3 Amplitude distribution function of a line object with size 2*w* located at a position $\xi = p$. 8

2.4 Block diagram for simulating hologram of multiple-line object. 13

2.5 (a) In-line hologram of three line objects and (b) its 1-D cross-sectional scan along the horizontal axis. 14

2.6 Amplitude distribution function of a square object with size 2*w* centered at $\xi = p_\xi$ and $\eta = p_\eta$. 15

2.7 Block diagram for simulating hologram of multiple-square object. 18

2.8 (a) In-line hologram of three square objects and (b) its 1-D cross-sectional scan along the horizontal axis. 19

2.9 Optical system for image reconstruction from the in-line hologram produces the twin images. 20

2.10 (a) Reconstructed image of a line object and (b) its 1-D cross-sectional scan. 22

2.11 Hologram recording with an off-axis reference beam. 23

2.12 Image reconstruction of a hologram recorded with off-axis reference beam. 23

2.13 Block diagram for computing numerical image reconstruction. 25

LIST OF FIGURES (Continued)

Figure **Page**

2.14 (a) Reconstructed image from the in-line hologram and (b) its 1-D cross-sectional scan. 26

3.1 In-line holograms of line object: (a) without modification, (b) with removal of the background, and (c) with the removal of the diverging wave. 1-D cross-sectional scans of: (d) the original hologram, (e) hologram with removal of the background, and (f) hologram with removal of the diverging wave. 29

3.2 Reconstructed images from the hologram of line object: (a) without modification, (b) with removal of the background, and (c) with removal of the diverging wave. 1-D cross-sectional scans of the corresponding reconstructed images: (d) without modification, (e) with the background removal, and (f) with the diverging wave removal. 30

3.3 PSNR of the image reconstructed from the hologram of a line object with size $2w$ = 125 μm as a function of the recording distance. 31

3.4 PSNR of the image reconstructed from the hologram of a line object with size $2w$ = 250 μm as a function of the recording distance. 31

3.5 1-D cross-sectional scans of the reconstructed image of line object with diameter (a) 125 μm and (b) 250 μm and their enlarged peaks shown in (c) Fig. 3.5(a) and (d) Fig. 3.5(b). 33

LIST OF FIGURES (Continued)

Figure **Page**

3.6 In-line holograms of square object: (a) without modification, (b) with removal of the background, and (c) with removal of the diverging wave. 1-D cross-sectional scans of: (d) original hologram, (e) hologram with removal of the background, and (f) hologram with removal of the diverging wave. 34

3.7 Reconstructed images from the hologram of square object: (a) without modification, (b) with removal of the background, and (c) with removal of the diverging wave. 1-D cross-sectional scans of the corresponding reconstructed images: (d) without modification, (e) with the background removal, and (f) with the diverging wave removal. 35

3.8 PSNR of the image reconstructed from the hologram of a square object with size $2w$ = 125 μm as a function of the recording distance. 36

3.9 PSNR of the image reconstructed from the hologram of a square object with size $2w$ = 250 μm as a function of the recording distance. 36

4.1 Geometrical distribution of multiple line objects separated by dz and $d\xi$ along the z and the ξ directions, respectively. 39

4.2 In line holograms of three line objects: (a) without modification, and (b) with the background removals. 1-D cross sectional scans of: (c) original hologram, and (d) modified hologram. 39

LIST OF FIGURES (Continued)

Figure **Page**

4.3 Reconstructed images from the holograms of three line objects: (a) without modification, and (b) with the background removals. 1-D cross-sectional scan of the corresponding images: (c) without modification, and (d) with the background removals. 40

4.4 PSNR of images reconstructed from the holograms of multiple line objects having diameter (a) 125 μm and (b) 250 μm with the separation $d\xi = 1$ mm and $dz = 0$ mm. 41

4.5 PSNR of images reconstructed from the hologram of 3 line objects having diameter 125 μm with the separations $d\xi$ = 0.5 mm and 1 mm as a function of the recording distance. 42

4.6 In line holograms of three square objects: (a) without modification, and (b) with the background removals. 1-D cross sectional scans of: (c) the original hologram, and (d) modified hologram. 43

4.7 Reconstructed images from the holograms of three square objects: (a) without modification, and (b) with the background removals. 1-D cross-sectional scan of the corresponding images: (c) without modification, and (d) with the background removals. 44

4.8 PSNR of images reconstructed from the hologram of multiple square objects having diameter (a) 125 μm and (b) 250 μm with separation $d\xi = 1$ mm and $dz = 0$ mm. 45

LIST OF FIGURES (Continued)

Figure **Page**

4.9 In line holograms of three line objects: (a) without modification, and (b) with the background removals. 1-D cross sectional scans of: (c) the original hologram, and (d) the modified hologram. 47

4.10 Reconstructed images from the hologram of three line objects: (a) without modification, and (b) with the background removals. 1-D cross sectional scans of the corresponding image: (c) without modification, and (d) with the background removals. 48

4.11 PSNR of the image reconstructed from the hologram of multiple line objects having diameter (a) 125 μm and (b) 250 μm with the separation $d\xi = 1$ and $dz = 1$ mm. 49

4.12 PSNR of the image reconstructed from the hologram of multiple line objects having diameter 125 μm with the separation dz = 0.5 mm and 1 mm. 50

4.13 In-line holograms of three square objects: (a) without modification, and (b) with the background removals. 1-D cross sectional scans of: (c) the original hologram, and (d) the modified hologram. 51

4.14 Reconstructed images from the holograms of three square objects: (a) without modification, and (b) with the background removals. 1-D cross-sectional scan of the corresponding images: (c) without modification, and (d) with the background removals. 52

LIST OF FIGURES (Continued)

Figure **Page**

4.15 PSNR of the image reconstructed from the hologram of multiple square objects having diameter (a) 125 μm and (b) 250 μm with the separation $d\xi = 1$ and $dz = 1$ mm. 53

ACKNOWLEDGEMENTS

I would like to express my gratitude to Assoc. Prof. Dr. Joewono Widjaja for his continuous guidance, help and encouragement throughout the course of this study. I am indebted to his valuable insights and constructive comments on my work. This thesis would not have reached completion without his constant encouragement and support.

I wish to express my special thank to Dr. Siriwat Soontaranon for his technical assistance throughout my research study.

Finally, I am indebted to my family for their love and encouragement throughout my studies.

Phacharawadee Raweng

Equation Chapter 1 Section 1CHAPTER I

INTRODUCTION

1.1 Background

In-line holography is a technique for recording an amplitude and a phase of light waves diffracted by a three dimensional (3-D) object onto photographic films (Hariharan, 1996). This technique is done by illuminating an object with a coherent light. An interference pattern between the diffracted wave and a reference wave is recorded on a photographic film, which is called an in-line hologram after a film development.

In order to reconstructs the recorded information, the developed hologram is illuminated with the same coherent reference wave. A wave diffracted from the hologram generates a real and virtual images of the original object behind and in front of the hologram, respectively. Consequently, the resultant reconstructed image is a superposition of the real image, the out-of-focus virtual image and the coherent background. As a result, the quality of the reconstructed is degraded. This is known as the twin image problem in the in-line holography.

In order to solve the twin image problem, the technique for separating the reference wave, which is added off-axis, from the object wave has been developed by Leith & Upatnieks (Leith and Upatnieks, 1962). However, this technique has a complex setup and requires high resolution films. The other technique is to record the hologram at a distance that satisfies a far-field condition (Thomson, 1963). In this case the virtual image become a weak background which can reduce the twin image

problem. This technique is limited to a small size of object. For large objects, a very long recording distance is required to satisfy the far-field condition which is impractical.

As technology of photodetector improves, digital recording of holograms by using a charge-couple device (CCD) sensor has been reported (Kreis, Adams and Jüptner, 1997; Soontaranon, Widjaja and Asakura, 2002; Pan and Meng, 2003; Soontaranon, Widjaja and Asakura, 2004). In comparison with the conventional holography, digital holography has advantages in that it is free from wet chemical development and either numerical reconstruction or signal processing can be used to retrieve the desired information. In the numerical reconstruction method, the amplitude and phase of the reconstructed image is retrieved by computing a Fresnel diffraction integral of the hologram at consecutive depths along the optical axis. As the case of the classical in-line holography, the numerical reconstruction generates the desired real image overlaid on the virtual image together with the strong coherent background. This twin image problem can be attributed to the loss of phase when the hologram was recorded. If the phase of the wave field incident on to the hologram plane were known, the problem can be solved. In order to find this phase information, phase retrieval algorithm has been proposed (Liu and Scott, 1987; Zhang, Pedrini, Osten and Tiziani, 2003). However, since the algorithm requires an iterative step, the drawback of this method is that a considerable number of iterations and computation time are required.

1.2 Significance of the study

As discussed in the preceding section, the degradation of the reconstructed image quality is caused by the interference pattern between the directly transmitted coherent background and the diverging wave associated with the virtual image. In order to solve this problem, the interference of pattern must be prevented from generating by eliminating either both or one of the unwanted wave fields. The elimination of the diverging wave is hard to be done, because the unknown phase information. As for the directly transmitted light, its elimination can be easily achieved by removing the uniform background of the hologram. In the case of the digital in-line hologram, the background can be determined by measuring an average of its intensity. By subtracting this average intensity from each pixel of the digital hologram, the directly transmitted wave is eliminated during the numerical reconstruction.

1.3 Research objective

The purpose of this thesis is to study the quality improvement of the reconstructed image from the digital in-line holograms by removing the uniform coherent background through computer simulation.

1.4 Scope and limitation of the study

In this thesis, 1-D and 2-D objects are used the test objects. The digital in-line holograms of single and multiple objects are simulated. After removing the background, the real image is numerically reconstructed. In order to verify the

feasibility of this method, the quality of the reconstructed image is quantitative measured by using a peak signal to noise ratio (PSNR) (Yang, Zhang and Mitra, 1999).

1.5 Organization

This thesis is organized into five chapters of which this is the first. Chapter II reviews the principles of the in-line holography. It starts with the formation of holograms multiple objects. The mathematical representations of the holograms of line and square objects and the image reconstruction with the present of twin image problem are discussed. In Chapter III, the elimination of twin image problem by removing the virtual image and the uniform coherent background from the in-line holograms of single object are studied. In Chapter IV, the quality improvement of the reconstructed image from the in-line holograms of multiple objects by using background removal is presented. Finally, the conclusions of this thesis are provided in Chapter V.

Equation Chapter 2 Section 1CHAPTER II

IN-LINE HOLOGRAPHY

2.1 Hologram formation

In-line holography is an optical method for recording amplitude and phase of coherent light wave diffracted by a three-dimensional (3-D) object on photographic film (Hariharan, 1996). This method was proposed by Dennis Gabor in 1948 in order to solve fundamental problem of conventional imaging systems which record only an intensity distribution of light wave. Since phase information of the wave field from different parts of objects is lost, a 3-D image reconstruction of objects cannot be obtained by the conventional imaging system. In order to preserve the phase information, the holographic method records an interference between the object wave

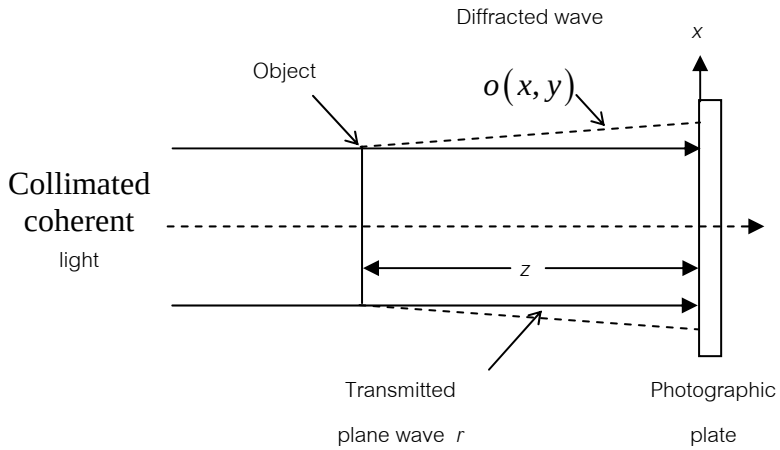

Figure 2.1 Optical system for recording an in-line (Gabor) hologram (Hariharan, 1996).

with a reference wave on a photographic film. After film development, the generated transparency is called a hologram.

In in-line holography, the object being studied is illuminated by a coherent wave as shown in Fig. 2.1. When the reference plane wave r and the object wave $o(x,y)$ are incident on a film placed at a distance z behind the object, the intensity of the recorded interference pattern can be expressed as

$$\begin{aligned} I(x,y) &= \left| r + o(x,y) \right|^2 \\ &= r^2 + \left| o(x,y) \right|^2 + r^* o(x,y) + r o^*(x,y), \end{aligned} \tag{2.1}$$

where $o^*(x,y)$ denotes complex conjugate of $o(x,y)$. The first term of Eq. (2.1) represents the uniform background recorded into the hologram. The second term is the intensity of the object wave. It can be seen that the third and the fourth terms preserve the amplitude and phase information of the object wave. Note that the developed film is referred to as a Gabor hologram or alternatively as an in-line hologram.

2.1.1 Hologram of Multiple-Objects

Figure 2.2 shows the hologram recording setup of multiple objects located at different distance. Light intensity at the recording plane can be mathematically expressed as

$$I(x,y) = \left| \sum_{i=1}^{n} \left\{ \frac{1}{n} \left(1 \otimes h_i\right) - \left(A_i \otimes h_i\right) \right\} \right|^2, \tag{2.2}$$

where A_i is the i^{th} object distribution while h_i is the free space propagation impulse response of the i^{th} object given by (Goodman, 1996)

$$h_i = \frac{\exp(jkz_i)}{j\lambda z_i}\exp\left\{ j\frac{k}{2z_i}\left(x^2 + y^2\right)\right\}. \tag{2.3}$$

The term $1 \otimes h$ and $-A \otimes h$ correspond to the reference and the object waves of Eq. (2.1), respectively. Here, the factor 1/*n* is introduced in order to normalize the amplitude of the reference wave such that its amplitude is always the same for any number of objects. Since the wave incident on each object emerges from the same source, thus, the relative phase of the wave propagations must be taken into account. If the plane where the object s_1 exists is used as a reference, the relative phase of the plane wave incident on the object s_2 and s_n can be expressed as $\exp(jk\Delta z_2)$ and $\exp(jk\Delta z_n)$, respectively. By taking this consideration into account, the impulse response corresponding to the i^{th} object can be expressed as

$$\begin{aligned} h_i(x,y) &= \frac{e^{jk(z_i+\Delta z_i)}}{j\lambda z_i}\exp\left\{ j\frac{k}{2z_i}\left(x^2 + y^2\right)\right\} \\ &= \frac{e^{jkz_1}}{j\lambda z_i}\exp\left\{ j\frac{k}{2z_i}\left(x^2 + y^2\right)\right\}. \end{aligned} \tag{2.4}$$

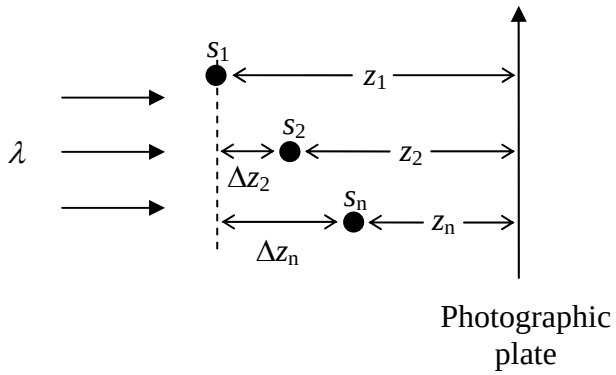

Figure 2.2 Schematic diagram of setup for recording hologram of three objects.

2.1.1.1 In-line hologram of multiple-line object

For a line object with size of $2w$ which is located at a position $\xi = p$ as shown in Fig. 2.3, its amplitude distribution function is defined as

$$A(\xi) = \begin{cases} 1 & \text{for } p - w \le \xi \le p + w \\ 0 & \text{otherwise.} \end{cases} \tag{2.5}$$

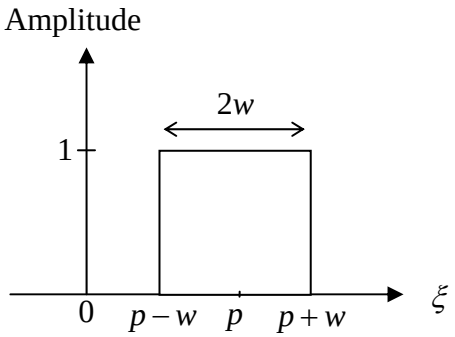

Figure 2.3 Amplitude distribution function of a line object with size $2w$ located at a position $\xi = p$.

When this object is illuminated by a plane wave with a wavelength λ, the object wave at the distance z can be derived as

$$\begin{aligned} -A \otimes h &= -\int_{-\infty}^{\infty}\int_{-\infty}^{\infty} A(\xi)\, h(x-\xi, y-\eta)\, d\xi d\eta \\ &= -\int_{-\infty}^{\infty}\int_{p-w}^{p+w} \frac{e^{jkz}}{j\lambda z} \exp\left\{\frac{j\pi}{\lambda z}\left\{(x-\xi)^2 + (y-\eta)^2\right\}\right\} d\xi d\eta \\ &= -\frac{e^{jkz}}{j\lambda z}\left[\int_{p-w}^{p+w} \exp\left\{\frac{j\pi}{\lambda z}(x-\xi)^2\right\} d\xi \int_{-\infty}^{\infty} \exp\left\{\frac{j\pi}{\lambda z}(y-\eta)^2\right\} d\eta\right]. \end{aligned} \tag{2.6}$$

By defining a new variable ξ' as

$$\xi' = \sqrt{\frac{2}{\lambda z}}(x - \xi)$$

and

$$d\xi = -\sqrt{\frac{\lambda z}{2}}d\xi',$$

the first integral of Eq. (2.6) can be rewritten as

$$\int_{p-w}^{p+w} \exp\left\{\frac{j\pi}{\lambda z}(x-\xi)^2\right\}d\xi = -\sqrt{\frac{\lambda z}{2}}\int_{\sqrt{2/\lambda z}(x-(p-w))}^{\sqrt{2/\lambda z}(x-(p+w))} \exp\left\{\frac{j\pi}{2}\xi'^2\right\}d\xi'$$

$$= -\sqrt{\frac{\lambda z}{2}}\int_{\sqrt{2/\lambda z}(x-p+w)}^{\sqrt{2/\lambda z}(x-p-w)} \left\{\cos\left(\frac{\pi\xi'^2}{2}\right) + j\sin\left(\frac{\pi\xi'^2}{2}\right)\right\}d\xi'$$

$$= -\sqrt{\frac{\lambda z}{2}}\left\{\int_{\sqrt{2/\lambda z}(x-p+w)}^{\sqrt{2/\lambda z}(x-p-w)} \cos\left(\frac{\pi\xi'^2}{2}\right)d\xi' + \int_{\sqrt{2/\lambda z}(x-p+w)}^{\sqrt{2/\lambda z}(x-p-w)} j\sin\left(\frac{\pi\xi'^2}{2}\right)d\xi'\right\}$$

$$= -\sqrt{\frac{\lambda z}{2}}\left\{\int_{\sqrt{2/\lambda z}(x-p+w)}^{0} \cos\left(\frac{\pi\xi'^2}{2}\right)d\xi' + \int_{0}^{\sqrt{2/\lambda z}(x-p-w)} \cos\left(\frac{\pi\xi'^2}{2}\right)d\xi'\right.$$

$$\left. + \int_{\sqrt{2/\lambda z}(x-p+w)}^{0} j\sin\left(\frac{\pi\xi'^2}{2}\right)d\xi' + \int_{0}^{\sqrt{2/\lambda z}(x-p-w)} j\sin\left(\frac{\pi\xi'^2}{2}\right)d\xi'\right\}$$

$$= -\sqrt{\frac{\lambda z}{2}}\left\{-\int_{0}^{\sqrt{2/\lambda z}(x-p+w)} \cos\left(\frac{\pi\xi'^2}{2}\right)d\xi' + \int_{0}^{\sqrt{2/\lambda z}(x-p-w)} \cos\left(\frac{\pi\xi'^2}{2}\right)d\xi'\right.$$

$$\left. - \int_{0}^{\sqrt{2/\lambda z}(x-p+w)} j\sin\left(\frac{\pi\xi'^2}{2}\right)d\xi' + \int_{0}^{\sqrt{2/\lambda z}(x-p-w)} j\sin\left(\frac{\pi\xi'^2}{2}\right)d\xi'\right\}. \quad (2.7)$$

According to the definition of the Fresnel integrals that (Goodman, 1996)

$$C(z) = \int_0^z \cos\left(\frac{\pi t^2}{2}\right)dt \quad (2.8a)$$

and

$$S(z) = \int_0^z \sin\left(\frac{\pi t^2}{2}\right)dt, \quad (2.8b)$$

Eq. (2.7) can be expressed as

$$\int_{p-w}^{p+w} \exp\left\{\frac{j\pi}{\lambda z}(x-\xi)^2\right\} d\xi = -\sqrt{\frac{\lambda z}{2}}\Big[-C\left\{\sqrt{2/\lambda z}\,(x-p+w)\right\} + C\left\{\sqrt{2/\lambda z}\,(x-p-w)\right\} - jS\left\{\sqrt{2/\lambda z}\,(x-p+w)\right\} + jS\left\{\sqrt{2/\lambda z}\,(x-p-w)\right\}\Big]. \quad (2.9)$$

In analogy, the second integral of Eq. (2.6) becomes

$$\int_{-\infty}^{\infty} \exp\left\{\frac{j\pi}{\lambda z}(y-\eta)^2\right\} d\xi = -\sqrt{\frac{\lambda z}{2}}\Big[-C(\infty)+C(-\infty) - jS(\infty)+jS(-\infty)\Big]. \quad (2.10)$$

Since the value of $C(\infty)=S(\infty)=\frac{1}{2}$ and $C(-\infty)=S(-\infty)=-\frac{1}{2}$ (Grashteyn and Ryzhik, 1994), Eq. (2.10) reduces to

$$\int_{-\infty}^{\infty} \exp\left\{\frac{j\pi}{\lambda z}(y-\eta)^2\right\} d\xi = -\sqrt{\frac{\lambda z}{2}}\left[-\left(\frac{1}{2}\right)+\left(-\frac{1}{2}\right)-\left(\frac{j}{2}\right)+\left(-\frac{j}{2}\right)\right] = -\sqrt{\frac{\lambda z}{2}}[-1-j]. \quad (2.11)$$

Substitutions of Eqs. (2.9) and (2.11) into Eq. (2.6) give

$$-A\otimes h = -\frac{e^{jkz}}{2j}[-1-j]\Big[-C\left\{\sqrt{2/\lambda z}\,(x-p+w)\right\} + C\left\{\sqrt{2/\lambda z}\,(x-p-w)\right\} - jS\left\{\sqrt{2/\lambda z}\,(x-p+w)\right\} + jS\left\{\sqrt{2/\lambda z}\,(x-p-w)\right\}\Big]. \quad (2.12)$$

Next, the reference wave can be calculated from

$$1\otimes h(x,y) = \int_{-\infty}^{\infty}\int_{-\infty}^{\infty} h(x-\xi, y-\eta)\,d\xi d\eta = \int_{-\infty}^{\infty}\int_{-\infty}^{\infty} \frac{e^{jkz}}{j\lambda z}\exp\left\{j\frac{k}{2z}\left\{(x-\xi)^2+(y-\eta)^2\right\}\right\} d\xi d\eta$$

$$= \frac{e^{jkz}}{j\lambda z}\int_{-\infty}^{\infty}\int_{-\infty}^{\infty}\exp\left\{\frac{j\pi}{\lambda z}\left\{(x-\xi)^2+(y-\eta)^2\right\}\right\}d\xi d\eta$$

$$= \frac{e^{jkz}}{j\lambda z}\left[\int_{-\infty}^{\infty}\exp\left\{\frac{j\pi}{\lambda z}(x-\xi)^2\right\}d\xi+\int_{-\infty}^{\infty}\exp\left\{\frac{j\pi}{\lambda z}(y-\eta)^2\right\}d\eta\right]. \quad (2.13)$$

By using the same steps used for deriving Eq. (2.6), the reference wave is found to be

$$1\otimes h(x,y) = \frac{e^{jkz}}{j\lambda z}\left(-\sqrt{\frac{\lambda z}{2}}\right)[-1-j]\left(-\sqrt{\frac{\lambda z}{2}}\right)[-1-j]$$

$$= e^{jkz}. \quad (2.14)$$

The in-line hologram of multiple line objects can be generated from Eq. (2.2) by using Eqs. (2.12) and (2.14). Thus, for three line objects, the recorded intensity of the hologram becomes

$$I(x,y) = \left|\sum_{i=1}^{3}\left\{\frac{1}{3}(1\otimes h_i)-(A_i\otimes h_i)\right\}\right|^2$$

$$= \left|\frac{1}{3}(1\otimes h_1)-(A\otimes h_1)+\frac{1}{3}(1\otimes h_2)-(A\otimes h_2)+\frac{1}{3}(1\otimes h_3)-(A\otimes h_3)\right|^2$$

$$= \left|\frac{1}{3}e^{jkz_1}-\frac{e^{jkz_1}}{2j}[-1-j]\left[-C\left\{\sqrt{2/\lambda z_1}(x-p_1+w)\right\}\right.\right.$$

$$+C\left\{\sqrt{2/\lambda z_1}(x-p_1-w)\right\}-jS\left\{\sqrt{2/\lambda z_1}(x-p_1+w)\right\}$$

$$\left.\left.+jS\left\{\sqrt{2/\lambda z_1}(x-p_1-w)\right\}\right]\right.$$

$$+\frac{1}{3}e^{jkz_1}-\frac{e^{jkz_2}}{2j}[-1-j]\left[-C\left\{\sqrt{2/\lambda z_2}(x-p_2+w)\right\}\right.$$

$$+C\left\{\sqrt{2/\lambda z_2}(x-p_2-w)\right\}-jS\left\{\sqrt{2/\lambda z_2}(x-p_2+w)\right\}$$

$$\left.+jS\left\{\sqrt{2/\lambda z_2}(x-p_2-w)\right\}\right]$$

$$+\frac{1}{3}e^{jkz_1}-\frac{e^{jkz_3}}{2j}[-1-j]\left[-C\left\{\sqrt{2/\lambda z_3}(x-p_3+w)\right\}\right.$$

$$+C\left\{\sqrt{2/\lambda z_3}\left(x-p_3-w\right)\right\}-jS\left\{\sqrt{2/\lambda z_3}\left(x-p_3+w\right)\right\}$$
$$+jS\left\{\sqrt{2/\lambda z_3}\left(x-p_3-w\right)\right\}\Big]\Big|^2 \qquad (2.15)$$

The block diagram in Fig. 2.4 shows the algorithm for generating the hologram of multiple-line object. The hologram is generated by computing the complex amplitude of the interference pattern between the reference and the individual object wave U_i. In order to achieve U_i, each object plane is prepared by constructing a zero matrix $\tilde{A}_i$ having dimension $N_x \times N_y$ pixels. For the line object oriented in the vertical direction, the number of pixels corresponding to the object size $2w$ is obtained by dividing $2w$ with the pixel size in horizontal direction T_x. The object distribution of the line object located at position $\xi = p_i$ is generated by defining the pixel value at all rows from the column $N_x/2+\left(p_i-w\right)/T_x$ to $N_x/2+\left(p_i+w\right)/T_x$ to be 1. Next, the impulse response at the desired recording distance z_i is generated by using Eq. (2.4). This computation uses the same size and the same number of pixels as those used in generating the object distribution. Then, the complex amplitude distribution at the recording plane U_i is calculated from

$$U_i = \frac{1}{n}\left(1 \otimes h_i\right) - \left(A_i \otimes h_i\right). \qquad (2.16)$$

The convolution is computed by using the convolution theorem of the Fourier transform defined as (Goodman, 1996)

$$A \otimes h = \int_{-\infty}^{\infty}\int_{-\infty}^{\infty} A(\xi,\eta)\, h(x-\xi, y-\eta)\, d\xi d\eta$$
$$= F^{-1}\left\{F\left\{A(\xi,\eta)\right\} F\left\{h(\xi,\eta)\right\}\right\}, \qquad (2.17)$$

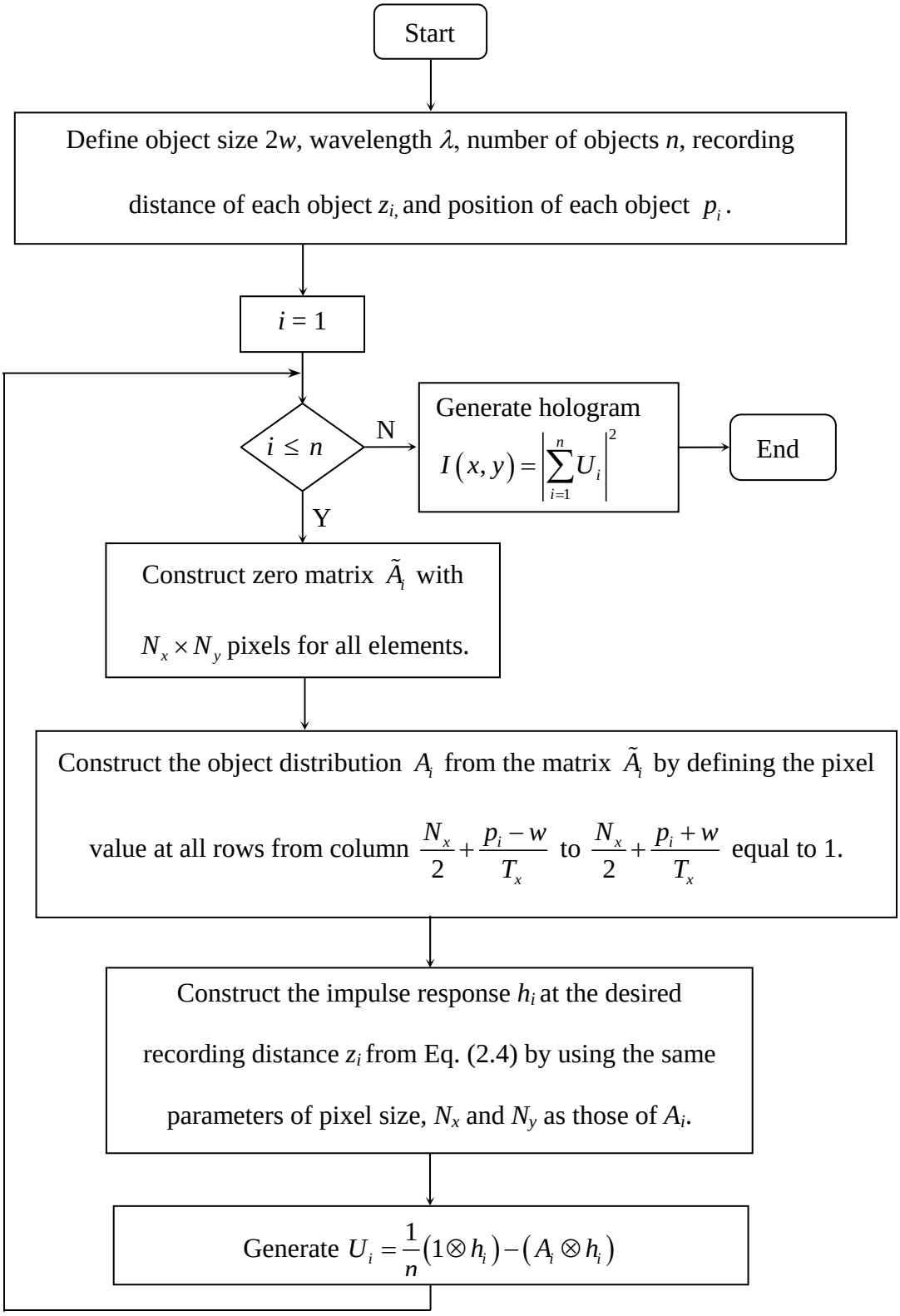

Figure 2.4 Block diagram for simulating hologram of multiple-line object.

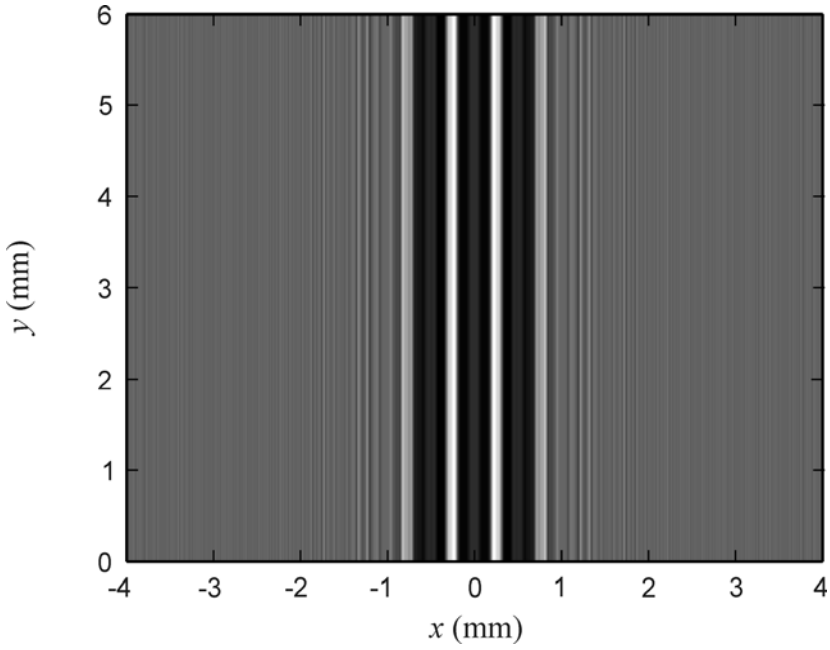

(a)

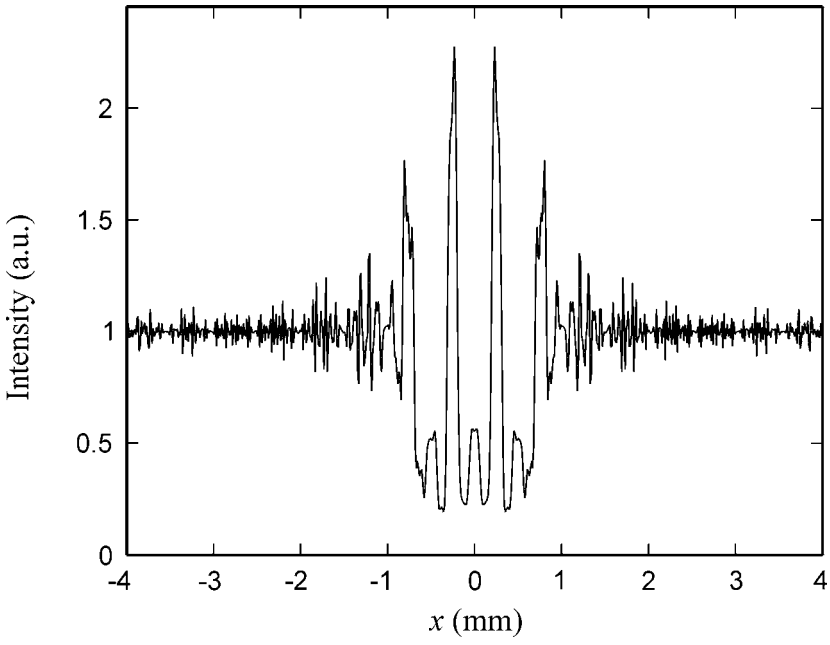

(b)

Figure 2.5 (a) In-line hologram of three line objects and (b) its 1-D cross-sectional scan along the horizontal axis.

where F is Fourier transform and F^{-1} is inverse Fourier transform. This process of generating U_i is repeated for every object. Finally, the hologram is obtained by taking a square modulus of the resultant summation of U_i. In this thesis, the number of pixels of the object plane in the x and the y directions are $N_x = 640$ and $N_y = 480$, respectively. Whereas the pixel size T_x is 12.5 μm. Figures 2.5(a) and (b) show the simulated in-line hologram of three identical line objects having size $2w$ = 125 μm and its 1-D cross-sectional scan. The objects are distributed in the same plane $(\Delta z = 0)$ with the horizontal separation of 0.5 mm. The recording distance of the objects is 10 cm and the wavelength of the illuminating light is λ = 632.8 nm. Since the separation of the object is very small, the hologram of one object is significantly disturbed by the others. As a result, the distortion of the hologram in Fig. 2.5(b) can be obviously observed.

2.1.1.2 In-line hologram of multiple-square object

In the case of a square object with size $2w$ centered at position $\xi = p_\xi$ and

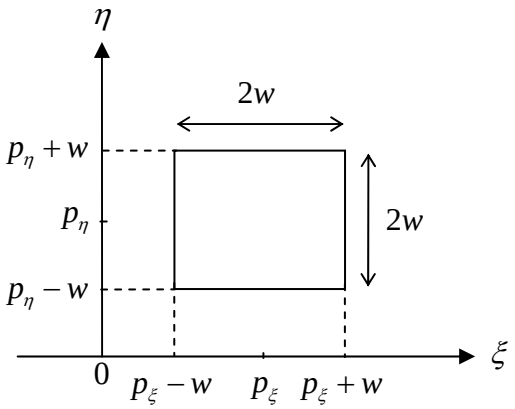

Figure 2.6 Amplitude distribution function of a square object with size $2w$ centered at $\xi = p_\xi$ and $\eta = p_\eta$.

$\eta = p_\eta$ as shown in Fig. 2.6, its amplitude distribution function is defined as

$$A(\xi,\eta) = \begin{cases} 1 & \text{for } p_\xi - w \le \xi \le p_\xi + w \text{ and } p_\eta - w \le \eta \le p_\eta + w \\ 0 & \text{otherwise.} \end{cases} \tag{2.18}$$

The object wave diffracted from this square object is found to be

$$\begin{aligned} -A \otimes h &= -\int_{-\infty}^{\infty}\int_{-\infty}^{\infty} A(\xi,\eta)\, h(x-\xi, y-\eta)\, d\xi d\eta \\ &= -\int_{p_\eta - w}^{p_\eta + w}\int_{p_\xi - w}^{p_\xi + w} \frac{e^{jkz}}{j\lambda z} \exp\left\{\frac{j\pi}{\lambda z}\left\{(x-\xi)^2 + (y-\eta)^2\right\}\right\} d\xi d\eta \\ &= -\frac{e^{jkz}}{j\lambda z}\left[\int_{p_\xi - w}^{p_\xi + w} \exp\left\{\frac{j\pi}{\lambda z}(x-\xi)^2\right\} d\xi \int_{p_\eta - w}^{p_\eta + w} \exp\left\{\frac{j\pi}{\lambda z}(y-\eta)^2\right\} d\eta\right]. \end{aligned} \tag{2.19}$$

By using the result from Eq. (2.9), Eq. (2.19) becomes

$$\begin{aligned} -A \otimes h = -\frac{e^{jkz}}{2j}\Big[& -C\left\{\sqrt{2/\lambda z}\left(x - p_\xi + w\right)\right\} + C\left\{\sqrt{2/\lambda z}\left(x - p_\xi - w\right)\right\} \\ & - jS\left\{\sqrt{2/\lambda z}\left(x - p_\xi + w\right)\right\} + jS\left\{\sqrt{2/\lambda z}\left(x - p_\xi - w\right)\right\}\Big] \\ & \times\Big[-C\left\{\sqrt{2/\lambda z}\left(y - p_\eta + w\right)\right\} + C\left\{\sqrt{2/\lambda z}\left(y - p_\eta - w\right)\right\} \\ & - jS\left\{\sqrt{2/\lambda z}\left(y - p_\eta + w\right)\right\} + jS\left\{\sqrt{2/\lambda z}\left(y - p_\eta - w\right)\right\}\Big]. \end{aligned} \tag{2.20}$$

Thus, in the case of three square objects, the hologram becomes

$$\begin{aligned} I(x,y) &= \left|\sum_{i=1}^{3}\left\{\frac{1}{3}(1 \otimes h_i) - (A_i \otimes h_i)\right\}\right|^2 \\ &= \left|\frac{1}{3}(1 \otimes h_1) - (A \otimes h_1) + \frac{1}{3}(1 \otimes h_2) - (A \otimes h_2) + \frac{1}{3}(1 \otimes h_3) - (A \otimes h_3)\right|^2 \end{aligned}$$

$$
\begin{aligned}
I(x,y) = \Bigg| & \frac{1}{3}e^{jkz_1} - \frac{e^{jkz_1}}{2j}\Big[-C\left\{\sqrt{2/\lambda z_1}\left(x - p_{\xi_1} + w\right)\right\} \\
& + C\left\{\sqrt{2/\lambda z_1}\left(x - p_{\xi_1} - w\right)\right\} - jS\left\{\sqrt{2/\lambda z_1}\left(x - p_{\xi_1} + w\right)\right\} \\
& + jS\left\{\sqrt{2/\lambda z_1}\left(x - p_{\xi_1} - w\right)\right\}\Big] \times \Big[-C\left\{\sqrt{2/\lambda z_1}\left(y - p_{\eta_1} + w\right)\right\} \\
& + C\left\{\sqrt{2/\lambda z_1}\left(y - p_{\eta_1} - w\right)\right\} - jS\left\{\sqrt{2/\lambda z_1}\left(y - p_{\eta_1} + w\right)\right\} \\
& + jS\left\{\sqrt{2/\lambda z_1}\left(y - p_{\eta_1} - w\right)\right\}\Big] \\
& + \frac{1}{3}e^{jkz_1} - \frac{e^{jkz_2}}{2j}\Big[-C\left\{\sqrt{2/\lambda z_2}\left(x - p_{\xi_2} + w\right)\right\} \\
& + C\left\{\sqrt{2/\lambda z_2}\left(x - p_{\xi_2} - w\right)\right\} - jS\left\{\sqrt{2/\lambda z_2}\left(x - p_{\xi_2} + w\right)\right\} \\
& + jS\left\{\sqrt{2/\lambda z_2}\left(x - p_{\xi_2} - w\right)\right\}\Big] \times \Big[-C\left\{\sqrt{2/\lambda z_2}\left(y - p_{\eta_2} + w\right)\right\} \\
& + C\left\{\sqrt{2/\lambda z_2}\left(y - p_{\eta_2} - w\right)\right\} - jS\left\{\sqrt{2/\lambda z_2}\left(y - p_{\eta_2} + w\right)\right\} \\
& + jS\left\{\sqrt{2/\lambda z_2}\left(y - p_{\eta_2} - w\right)\right\}\Big] \\
& + \frac{1}{3}e^{jkz_1} - \frac{e^{jkz_3}}{2j}\Big[-C\left\{\sqrt{2/\lambda z_3}\left(x - p_{\xi_3} + w\right)\right\} \\
& + C\left\{\sqrt{2/\lambda z_3}\left(x - p_{\xi_3} - w\right)\right\} - jS\left\{\sqrt{2/\lambda z_3}\left(x - p_{\xi_3} + w\right)\right\} \\
& + jS\left\{\sqrt{2/\lambda z_3}\left(x - p_{\xi_3} - w\right)\right\}\Big] \times \Big[-C\left\{\sqrt{2/\lambda z_3}\left(y - p_{\eta_3} + w\right)\right\} \\
& + C\left\{\sqrt{2/\lambda z_3}\left(y - p_{\eta_3} - w\right)\right\} - jS\left\{\sqrt{2/\lambda z_3}\left(y - p_{\eta_3} + w\right)\right\} \\
& + jS\left\{\sqrt{2/\lambda z_2}\left(y - p_{\eta_2} - w\right)\right\}\Big]\Bigg|^2
\end{aligned}
\tag{2.21}
$$

Figure 2.7 shows a block diagram for simulating the in-line hologram of multiple-square object by using Eq. (2.21). The process is similar to the case of the multiple-line object except that the object distribution function of square object is generated. The simulated hologram of three identical square objects having size $2w$ = 250 μm is illustrated in Fig. 2.8(a), while its 1-D cross-sectional scan is plotted in Fig. 2.8(b). The positions of the objects along the horizontal axis are $p_{\xi 1}$ = -1 mm, $p_{\xi 2}$ = 0 mm

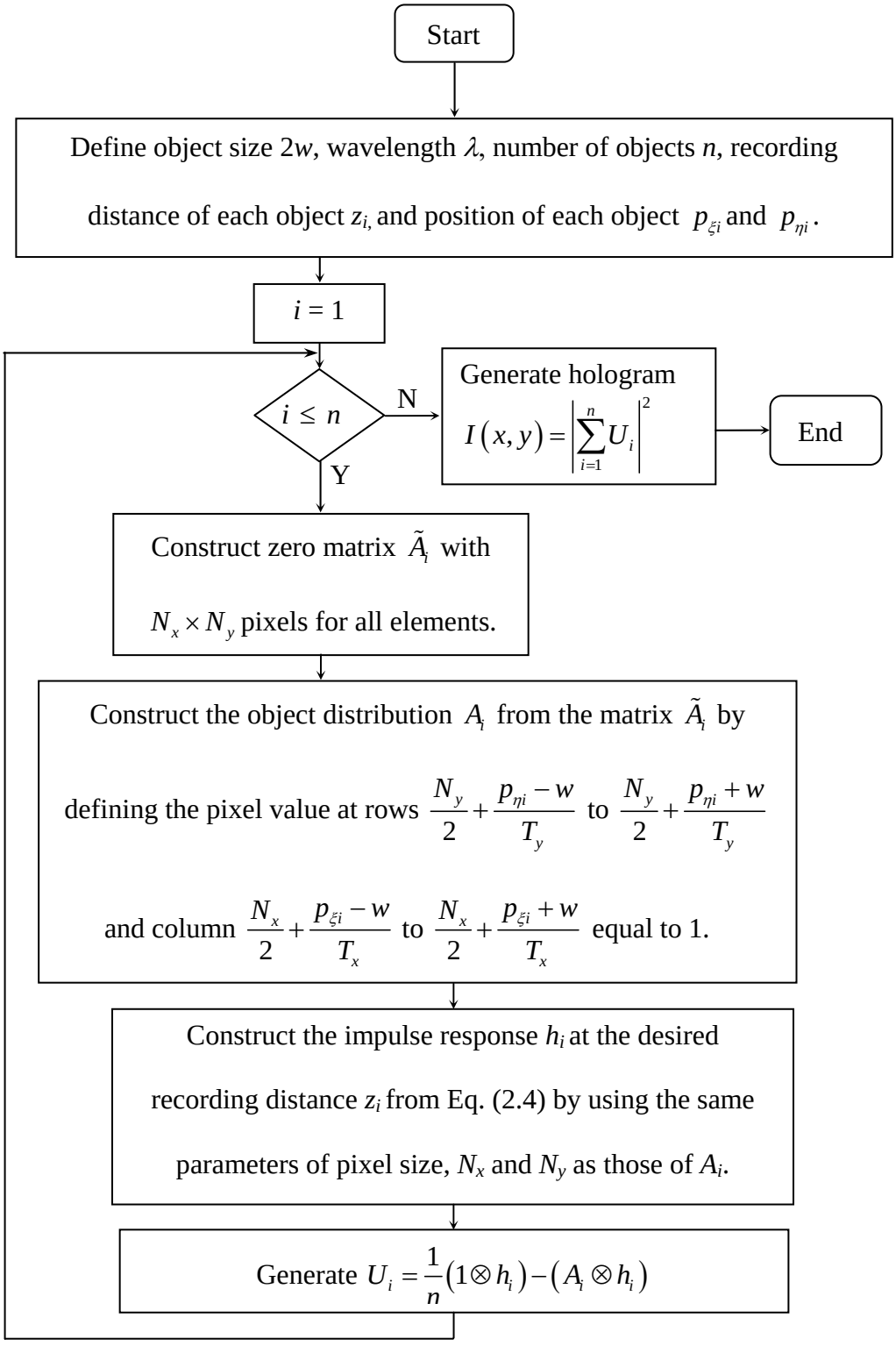

Figure 2.7 Block diagram for simulating hologram of multiple-square object.

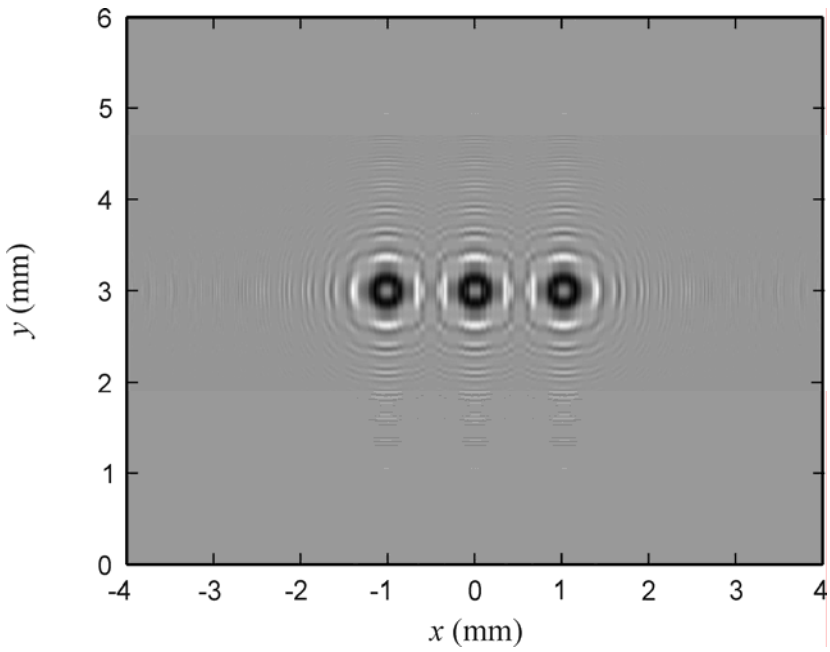

(a)

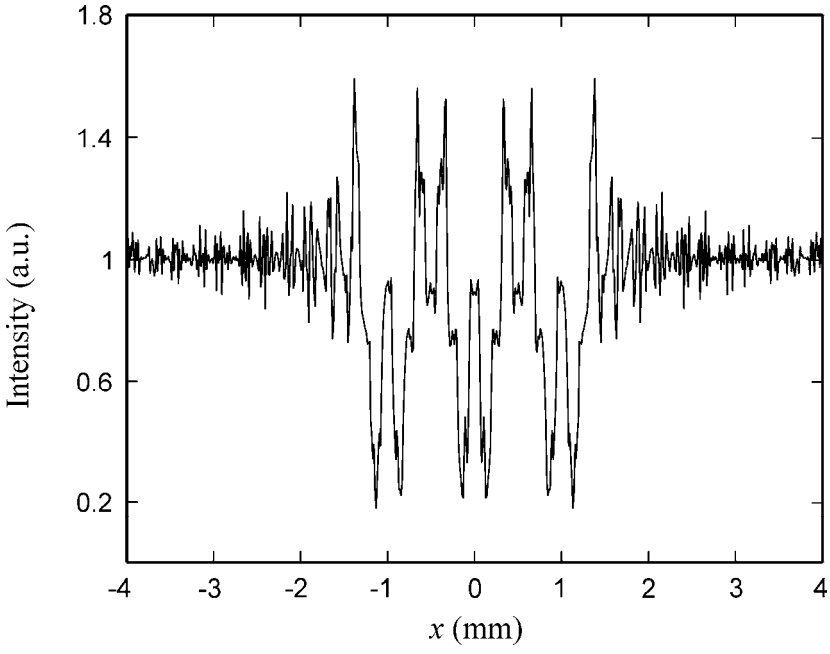

(b)

Figure 2.8 (a) In-line hologram of three square objects and (b) its 1-D cross-sectional scan along the horizontal axis.

and $p_{\xi 3}$ = 1 mm, while p_{η} is zero. They are distributed in the same plane $(\Delta z = 0)$ with distance z = 10 cm. The wavelength of the coherent source is 632.8 nm. As in the case of multiple-line object, the distortion of the hologram can be clearly observed due to the small separation of the objects.

2.2 Image reconstruction

In order to perform image reconstruction, the developed film with the amplitude transmittance given by Eq. (2.2) is illuminated with the same coherent reference wave as shown in Fig. 2.9. The reconstructed optical field immediately behind the hologram is

$$\begin{aligned} u(x,y) &= rI(x,y) \\ &= r^3 + r|o(x,y)|^2 + r^2 o(x,y) + r^2 o^*(x,y). \end{aligned} \tag{2.22}$$

The first term of Eq. (2.22) represents the directly transmitted coherent background. The second term corresponds to the intensity of the object wave. It is negligible, because the amplitude of the object wave is smaller than the reference wave

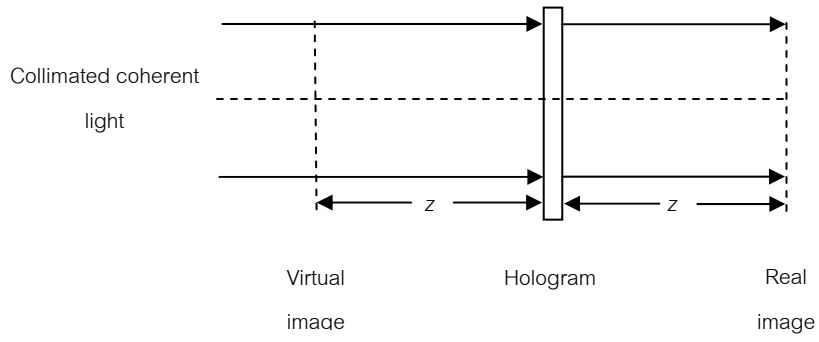

Figure 2.9 Optical system for image reconstruction from the in-line hologram produces the twin images (Hariharan, 1996).

$|o(x,y)|^2 r(x,y)$. The third term produces the first wave component that is the diverging wave, because it is diffracted by the object during recording of the hologram. This wave field image appears in front of the hologram, it is called a virtual image. The fourth term corresponds to the second wave component that is the conjugate of the original diffracted wave. This wave converges to form a conjugate twin image of the object at a distance *z* behind the hologram. This twin image is real.

Since the coherent background, the virtual and the real images are reconstructed on the same optical axis, overlapping of the images with the background can be seen by observing through the hologram toward the illuminating source. As the observer focuses on the real image, that is the desired information, the out-of-focus virtual image is also present. This is known as the twin image problem in the in-line holography. As the reconstructed wave field is detected by using photodetectors placed at the real-image plane, the real image is degraded by an interference pattern produced by the directly transmitted plane wave and the out-of-focus wave (Tyler and Thompson, 1976). Figure 2.10(a) shows the reconstructed image from the hologram of single line object, while its 1-D cross-sectional scan is illustrated in Fig. 2.10(b). Since the real image is proportional to the multiplication between the first term and the complex conjugate of the second term of Eq. (2.2) which has negative value, the intensity distribution of the reconstructed real image in Fig. 2.10(b) has the lowest value or a contrast reversal. The virtual image appeared at the original position of the object produces a diffraction pattern at the real image plane. The interference pattern between this diffracted wave and the directly transmitted light overlaps with the real image.

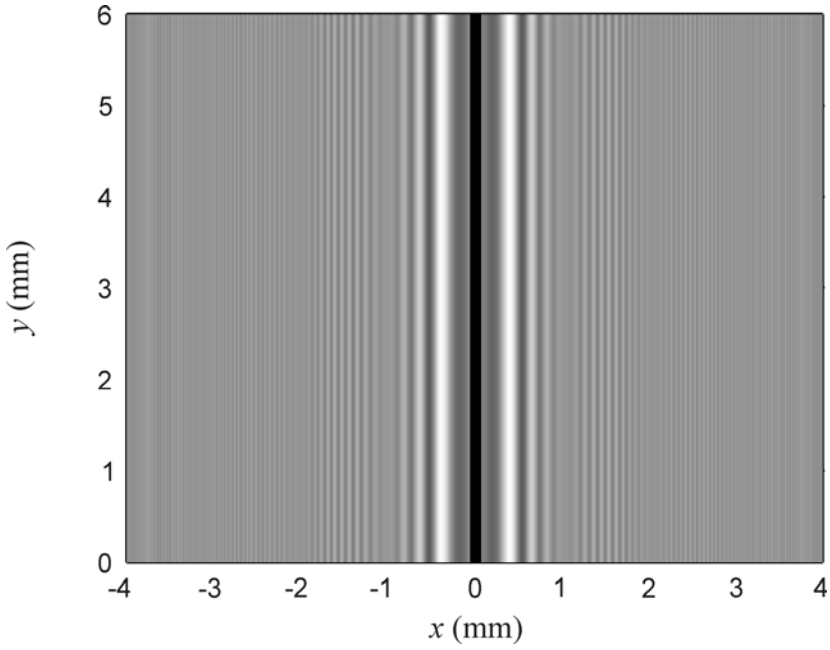

(a)

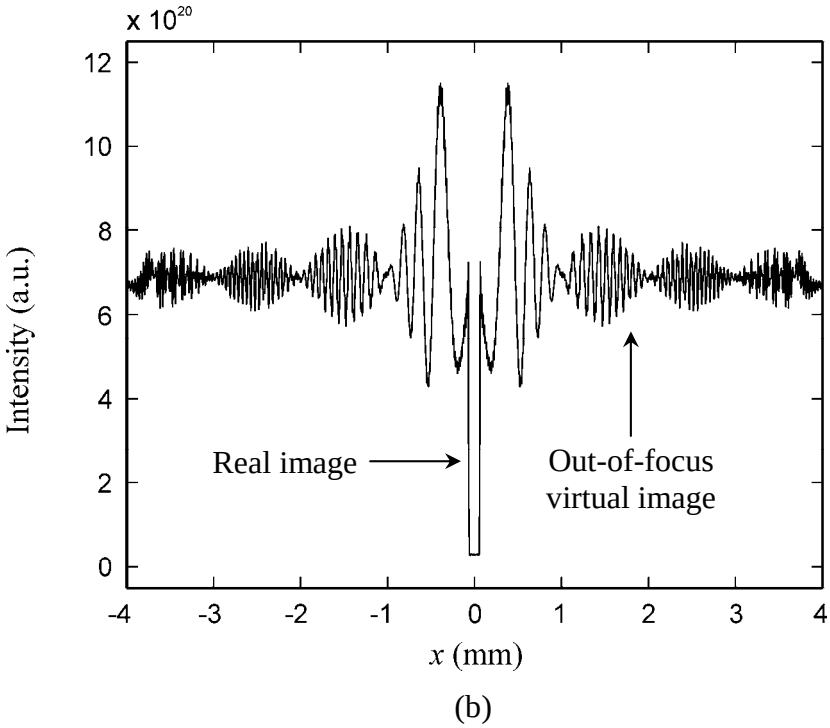

(b)

Figure 2.10 (a) Reconstructed image of a line object and (b) its 1-D cross-sectional scan.

In order to solve the twin image problem, an off-axis holography has been proposed by Leith and Upatnieks in 1962. Figure 2.11 shows a schematic diagram of an optical setup for implementing the off-axis holography. In this technique, the reference and the object waves originated from the same coherent source propagate in different direction and interfere at angle θ in the recording plane. In the reconstruction process, the reconstructed field is appeared to originate from the virtual and the real

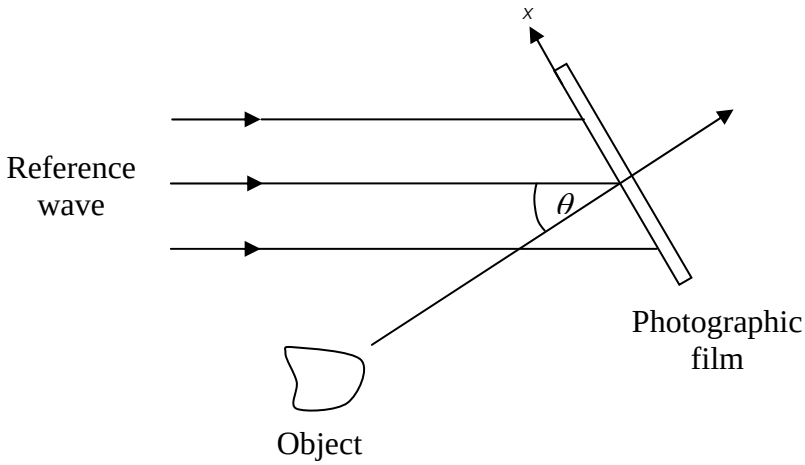

Figure 2.11 Hologram recording with an off-axis reference beam (Hariharan, 1996).

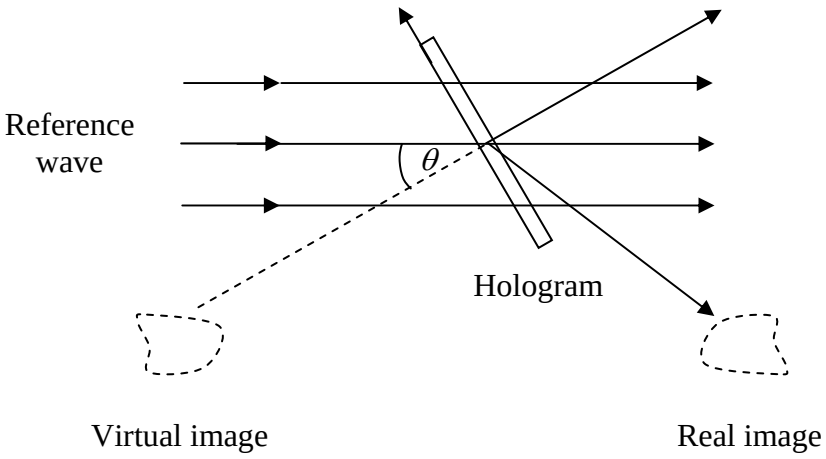

Figure 2.12 Image reconstruction of a hologram recorded with off-axis reference beam (Hariharan, 1996).

images located at the positions shown in Fig. 2.12. As a result, the real and the virtual images are separated from each other. Thus, the twin image problem does not occur. However, the optical setup for implementing the off-axis holography is complicated. Moreover, when the two waves interfere at angle θ, the resultant interference pattern has a fringe spacing δ given by (Kreis, Adams and Jüptner, 1997)

$$\delta = \frac{\lambda}{2\sin(\theta/2)}. \tag{2.23}$$

Since the fringe spacing δ is inverse proportional to the angle θ, the spacing reduces as the angle θ increases. Thus this technique requires high resolution photographic films.

By still maintaining the in-line geometry which is simpler than the off-axis setup, several techniques for eliminating the unwanted wave field have been proposed. One of the proposed techniques consider that objects to be studied must be very small, so that the recording distance satisfies the far-field condition defined by (Goodman, 1996)

$$z \gg \frac{k\left(\xi^2 + \eta^2\right)_{\max}}{2}, \tag{2.24}$$

where $\xi_{\max}$ and $\eta_{\max}$ are the object's maximum dimension in the horizontal and the vertical directions, respectively. As the recording distance satisfies Eq. (2.24), the generated hologram is called as the in-line Fraunhofer hologram. For the line object having the radius w = 62.5 μm and the illuminating coherent light operating at wavelength λ = 632.8 nm, the required far field distance is found to be $z \gg$ 7.76 cm. Figure 2.13 shows a block diagram for reconstructing images from the holograms.

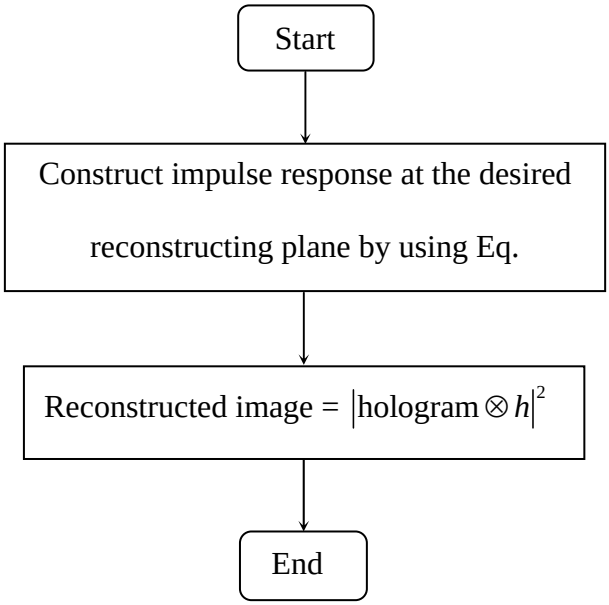

Figure 2.13 Block diagram for computing numerical image reconstruction.

First, the impulse response at the desired recording plane is generated by using Eq. (2.4). Then, the reconstructed image can be computed by taking a square modulus of the convolution between the hologram and the generated impulse response. The convolution is computed in accordance with Eq. (2.3). Figures 2.14(a) and (b) show the reconstructed image and its 1-D cross-sectional scan from the in-line Fraunhofer hologram. It is obvious that the amplitude of the virtual image shown in the Fig. 2.14(b) is much smaller that of the Fig. 2.10(b). Thus the virtual image reconstructed from the Fraunhofer hologram produces a weak background. Thus its disturbance to the real image decreases. However, a longer recording distance is required for a larger object size. This can be regarded as a limitation of the in-line Fraunhofer holography since the optical setup becomes impractical (Pitlak, Page and Selvin, 1976).

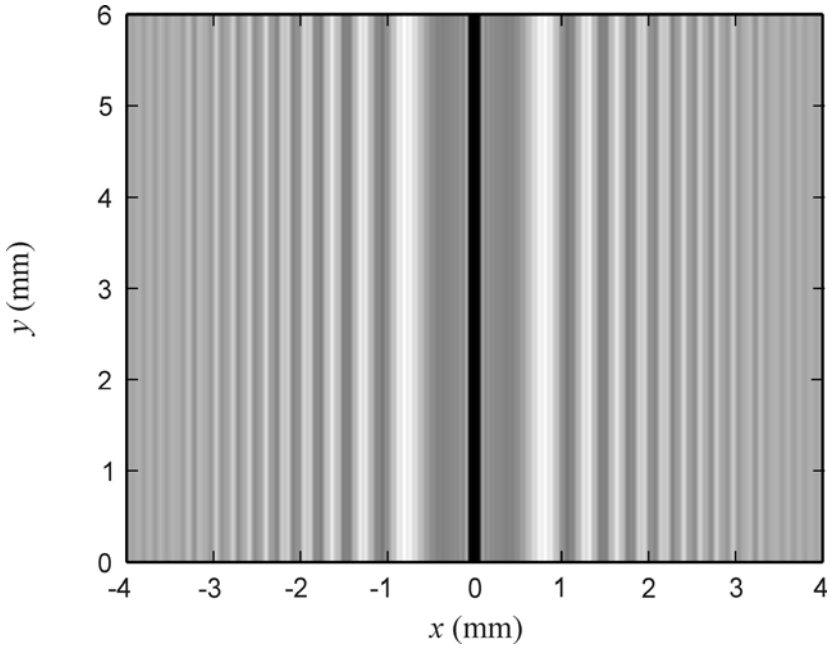

(a)

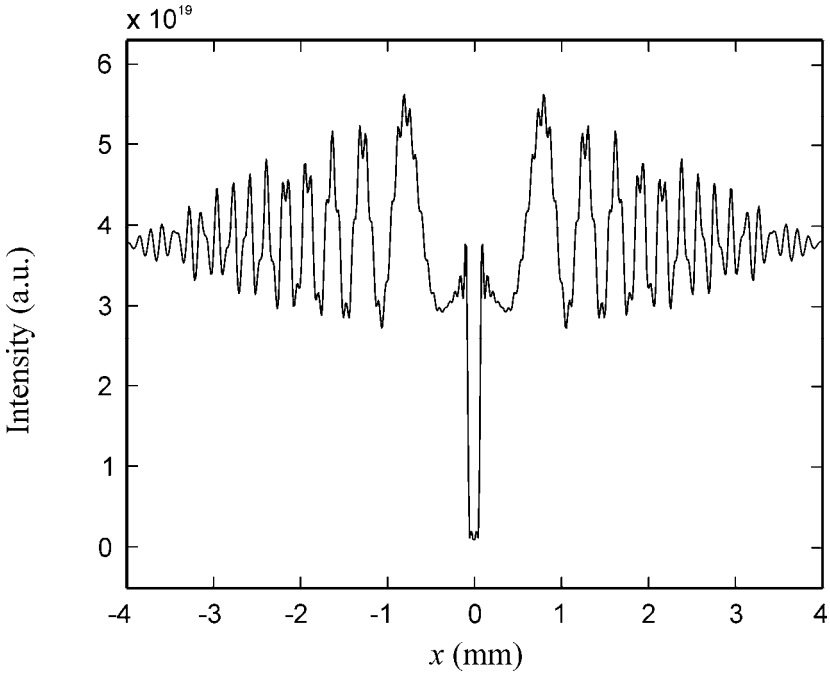

(b)

Figure 2.14 (a) Reconstructed image from the in-line hologram and (b) its 1-D cross-sectional scan.

2.3 Reduction of twin image problem by removing the uniform background

Since the out-of-focus virtual image at the reconstructing plane is generated from the interference between the directly transmitted plane wave and the wave diffracted from the virtual image. It can be eliminated as either one or all of these waves are removed. However, the elimination of the virtual image is hard to be done, because of the unknown phase information. As for the directly transmitted light, its elimination can be easily achieved by removing the uniform background of the hologram. The background can be determined by measuring an average of the hologram intensity. By subtracting this average intensity from the hologram, the directly transmitted wave is eliminated during the reconstruction process. In order to determine the quality of the images reconstructed from the holograms with background removal, a peak signal to noise ratio (PSNR) defined as (Yang, Zhang and Mitra, 1999)

$$\mathrm{PSNR} = 10\log_{10}\left\{\frac{1}{mn}\frac{\sum_{i=0}^{m-1}\sum_{j=0}^{n-1}\left[f\left(x_{ij},y_{ij}\right)-\hat{f}\left(x_{ij},y_{ij}\right)\right]^2}{f_{max}^2\left(x,y\right)}\right\}^{-1}, \qquad (2.25)$$

is employed. Here, $f\left(x,y\right)$ and $\hat{f}\left(x,y\right)$ are the original and the reconstructed images, respectively. $m \times n$ are the image size, while $f_{\max}\left(x,y\right)$ is the maximum attainable gray level value of the image pixel. The value of PSNR determines degree of similarity between two images. The larger PSNR value, the higher the quality of the reconstructed image.

CHAPTER III

IMAGE RECONSTRUCTIONS FROM IN-LINE HOLOGRAMS OF SINGLE OBJECT

According to Eq. (2.22), the reconstructed optical field consists mainly of the coherent background, the diverging and the converging waves. At the reconstruction plane the real image intensity generated by the converging wave is degraded by the interference pattern of the coherent background and the diverging wave. In order to improve the real image quality, either one or all of these waves must be removed. In this chapter, the effects of removal of the coherent background and of the converging wave from the hologram of a single line and square objects are studied through computer simulation.

3.1 Removal of virtual image and uniform background from holograms

In order to remove the coherent background from the in-line holograms defined by Eq. (2.1), the average intensity of the hologram is digitally calculated by

$$H_m = \frac{1}{NM}\sum_{k=0}^{N-1}\sum_{l=0}^{M-1} H\left(k\Delta x, l\Delta y\right), \tag{3.1}$$

where N and M are the number of pixels, while Δx and Δy are their corresponding pixel size in the horizontal and the vertical directions, respectively. Here, H represents the intensity distribution of the hologram. The background removal is then done by

subtracting this average intensity from the holograms. However, since the complex amplitude of the virtual image cannot be easily obtained from the hologram, the removal of the diverging wave is done by simulating the holograms without the third term of Eq. (2.1). The real images are numerically reconstructed from the modified holograms based on the block diagram shown in Fig. 2.15.

Figure 3.1(a) show the in-line hologram of line object with a size of 125 μm which is simulated at the recording distance z = 40 cm and the wavelength λ = 632.8 nm, while Figs. 3.1(b) and (c) are those without the coherent background and the diverging wave, respectively. Their 1-D cross-sectional scan are shown in Figs. 3.1(d), (e) and (f), respectively. Figures 3.2(a), (b) and (c) show the images

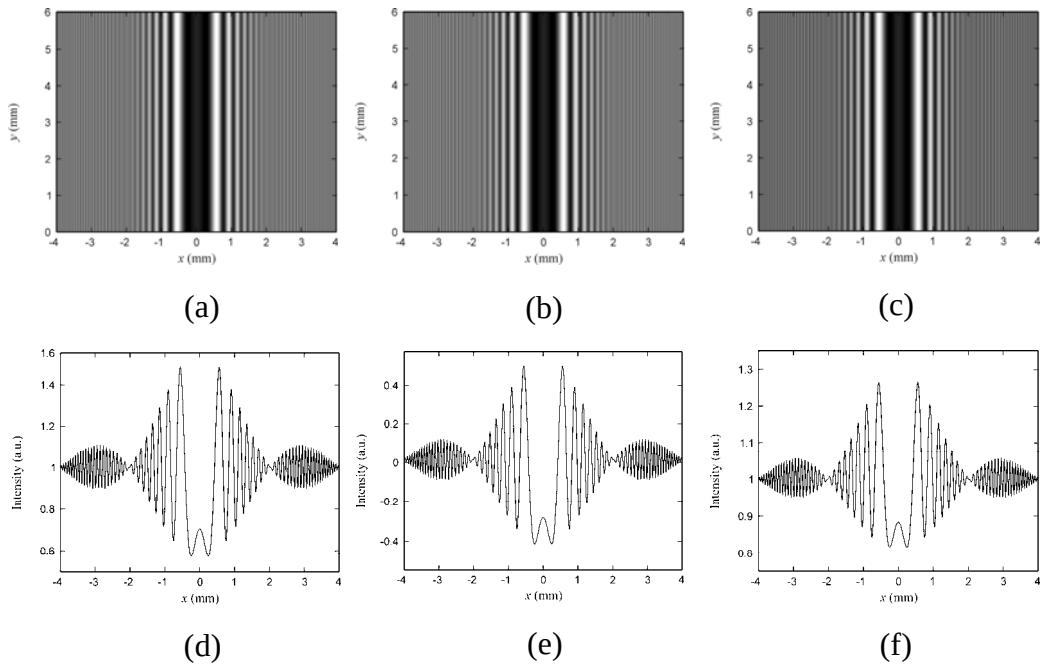

Figure 3.1 In-line holograms of line object: (a) without modification, (b) with removal of the background, and (c) with the removal of the diverging wave. 1-D cross-sectional scans of: (d) the original hologram, (e) hologram with removal of the background, and (f) hologram with removal of the diverging wave.

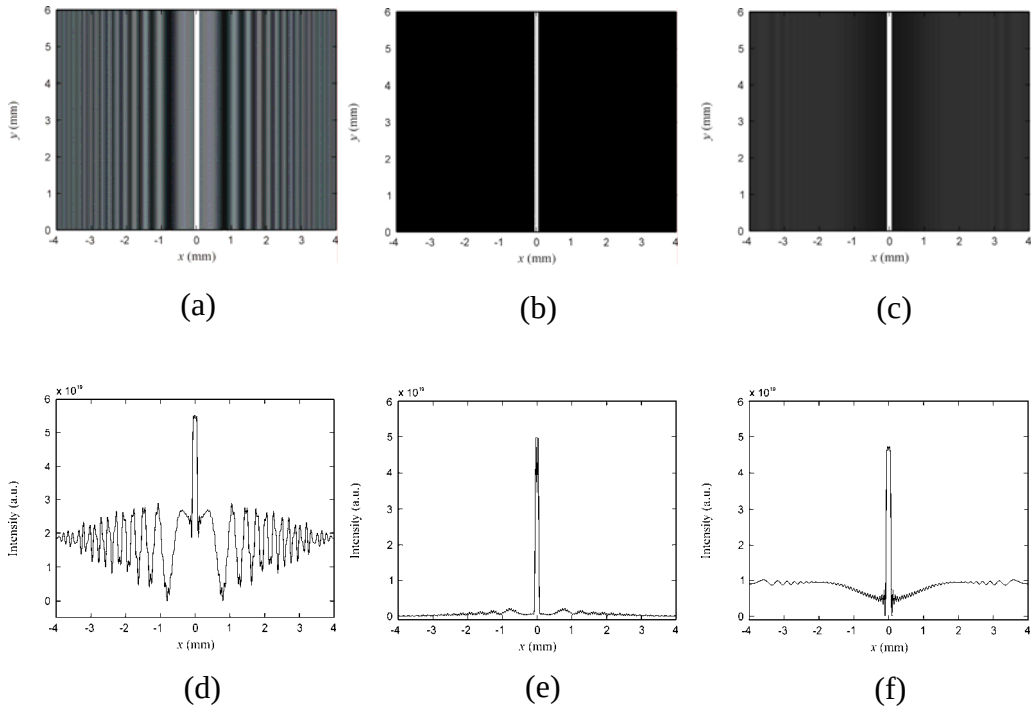

Figure 3.2 Reconstructed images from the hologram of line object: (a) without modification, (b) with removal of the background, and (c) with removal of the diverging wave. 1-D cross-sectional scans of the corresponding reconstructed images: (d) without modification, (e) with the background removal, and (f) with the diverging wave removal.

reconstructed from the corresponding in-line hologram shown in Fig. 3.1, while their 1-D cross-sectional scan are shown in Figs. 3.2(d), (e) and (f), respectively. Here, the contrast of image reconstructed from the original hologram shown in Fig. 3.2(d) is reversed by subtracting the maximum intensity from the reconstructed image. This is to compensate for the contrast reversal nature of the reconstructed image from in-line hologram in which the object wave is determined by negative value of the object distribution function. It can be seen from this figure that the desired image is overlapped by the unwanted interference pattern resulted from the out-of-focus virtual image. However, the removal of the coherent background and the diverging wave

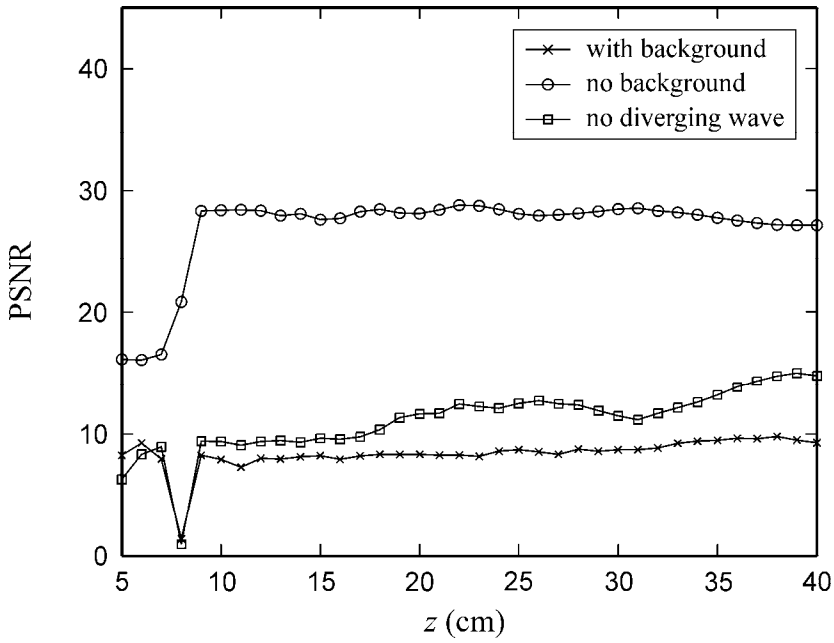

Figure 3.3 PSNR of the image reconstructed from the hologram of a line object with size $2w$ = 125 μm as a function of the recording distance.

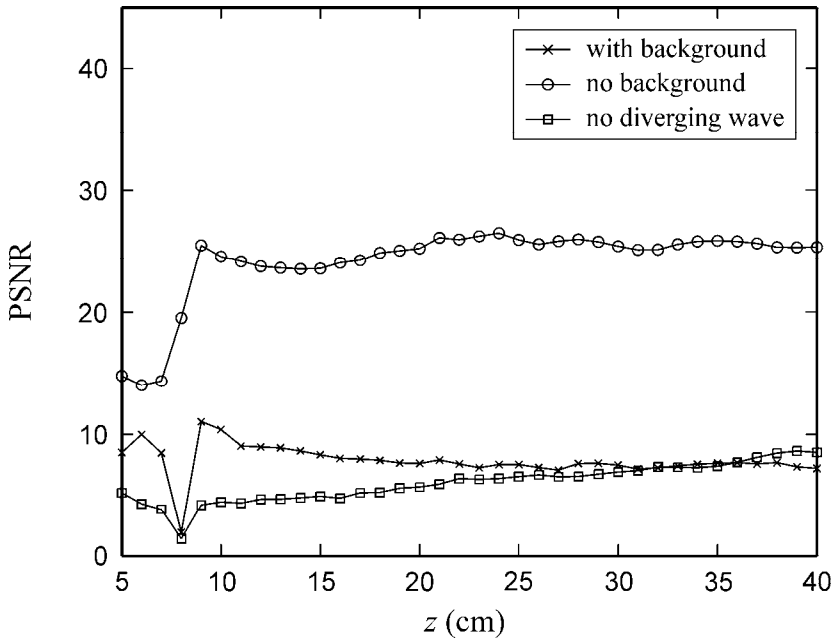

Figure 3.4 PSNR of the image reconstructed from the hologram of a line object with size $2w$ = 250 μm as a function of the recording distance.

could significantly suppress this interference pattern.

The PSNRs of the images reconstructed from the holograms of the line object by using the conventional technique with contrast reversal, the background and the diverging wave removals are represented in Fig. 3.3 as the cross, the circle and the square symbols, respectively. In this work, the holograms are generated at the recording distance z between 5 cm to 40 cm with the interval of $\Delta z = 0.5$ cm. Due to the present of the dc background in Fig. 3.2(f), the PSNR of the reconstructed images generated from the holograms without the diverging wave is smaller than that from the holograms without the uniform background.

Figure 3.4 shows the PSNR of the reconstructed images from the modified holograms of a bigger line object. Although the background removal gives higher PSNR than the diverging wave removal, the PSNR of the reconstructed image of the bigger object is lower than that of the smaller one. The reason for this is that first the ringing effect caused by the coherent optical system occurs at a whole area of the object image. This can be clearly seen from Figs. 3.5(a) and (b) which show the 1-D intensity profiles of the images of a line object having diameter 125 mm and 250 mm reconstructed using the background removal. The enlarged figure of the corresponding peak, while their profiles are illustrated in Figs. 3.5(c) and (d), respectively. It can be seen that the larger object contains longer fluctuation than the smaller one. As a result, it gives smaller PSNR. Second, according to Tyler (Tyler and Thomson, 1976), the amplitude of the interference pattern which determines the amplitude of reconstructed virtual and real images is proportional to the object size. As a result, the larger object size gives a stronger out-of-focus virtual image.

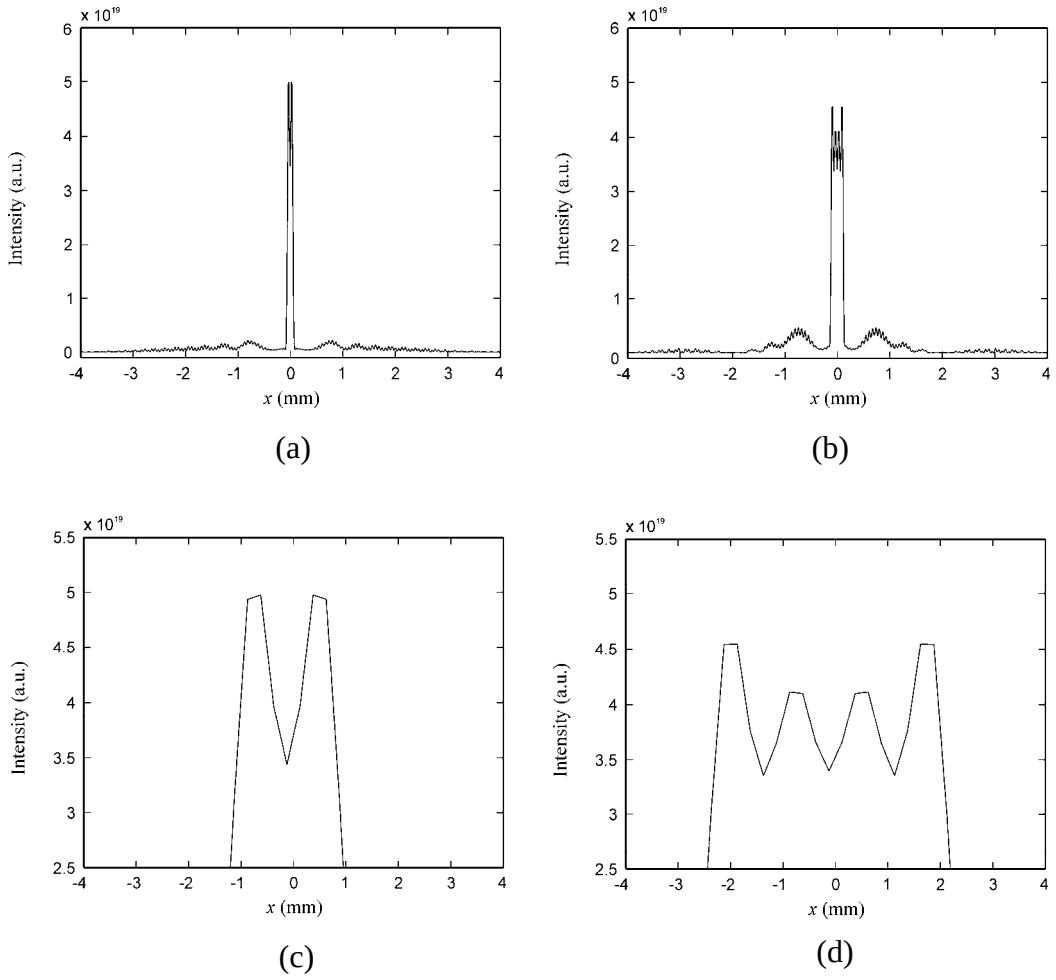

Figure 3.5 1-D cross-sectional scans of the reconstructed image of line object with diameter (a) 125 μm and (b) 250 μm and their enlarged peaks shown in (c) Figs. 3.5(a) and (d) Fig. 3.5(b).

Therefore, the image reconstructed from the hologram of a smaller object size gives higher PSNR than that of the large object. Furthermore, the sharp decrease of the PSNR in Figs. 3.3 and 3.4 at distance smaller than 7 cm may be caused by the fact that the frequency of the interference pattern of the hologram is inverse proportional to the recording distance. At a short recording, frequency of the interference pattern is very high such that the hologram is under sampled.

As for the square object having size of 125 μm, the in-line hologram which is simulated at the recording distance z = 40 cm and the wavelength λ = 632.8 nm is shown in Fig. 3.6(a), while Figs. 3.6(b) and (c) are those without the coherent background and the diverging wave, respectively. Their 1-D cross-sectional scan are shown in Figs. 3.6(d), (e) and (f), respectively. Figures 3.7(a), (b) and (c) show the images reconstructed from the corresponding in-line hologram shown in Fig. 3.6, while their 1-D cross-sectional scan are shown in Figs. 3.7(d), (e) and (f), respectively. In comparison with Fig. 3.2(d), the unwanted interference fringes shown in Fig. 3.7(d) is smaller. In analogy with the case of the line object, the out-of-focus virtual images are reduced significantly from both modified holograms.

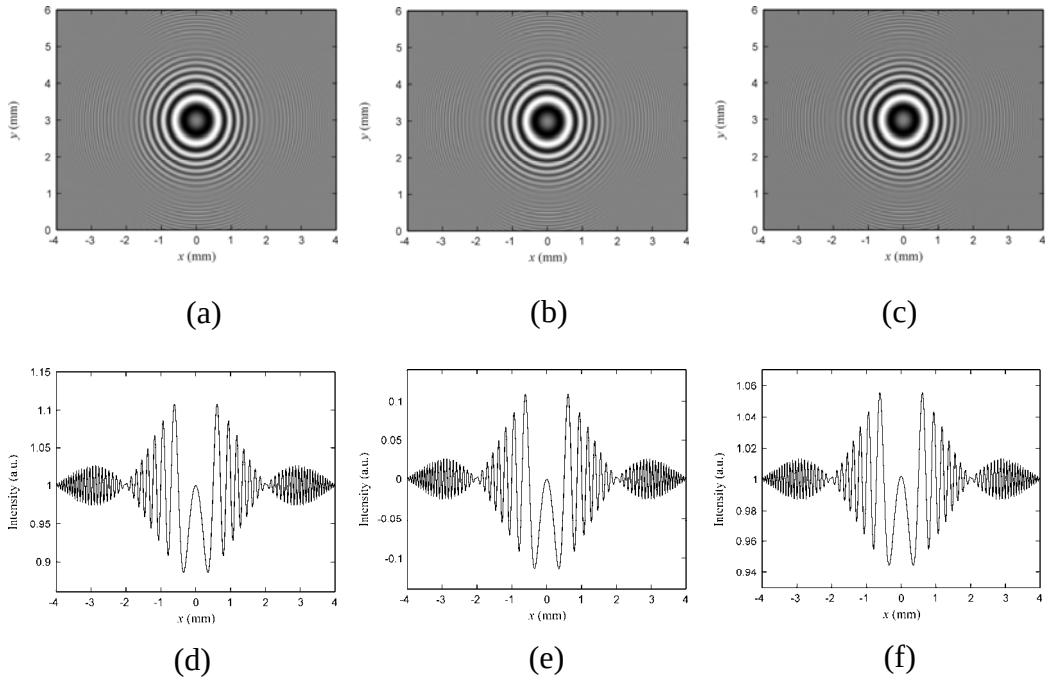

Figure 3.6 In-line holograms of square object: (a) without modification, (b) with removal of the background, and (c) with removal of the diverging wave. 1-D cross-sectional scans of: (d) original hologram, (e) hologram with removal of the background, and (f) hologram with removal of the diverging wave.

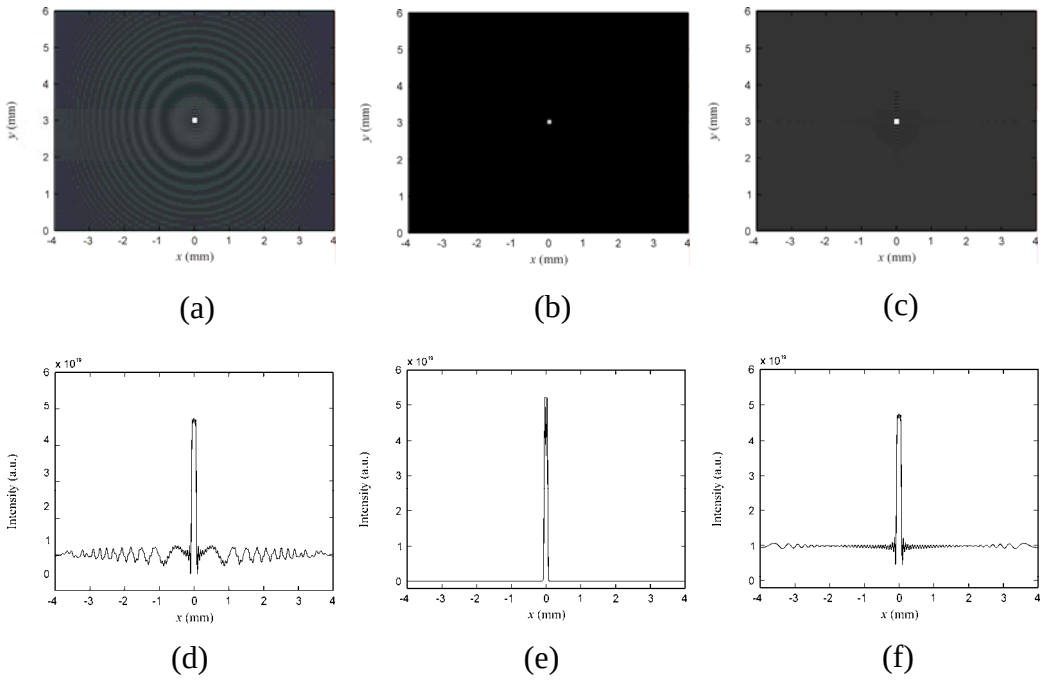

Figure 3.7 Reconstructed images from the hologram of square object: (a) without modification, (b) with removal of the background, and (c) with removal of the diverging wave. 1-D cross-sectional scans of the corresponding reconstructed images: (d) without modification, (e) with the background removal, and (f) with the diverging wave removal.

Figures 3.8 and 3.9 show the PSNR of the reconstructed images from the modified holograms of a square object having the size w of 62.5 μm and 125 μm, respectively. The same tendencies as the case of the line object are observed that are the dc removal gives higher PSNR than that of the virtual image removal, and the larger object gives lower PSNR than that of the small object. In the case of the square object, the background intensity in Fig. 3.7(e) is smoother than that of the line object in Fig. 3.2(e). This may be caused by the fact that the amplitude of the light wave diffracted from the square object is smaller than that of the line object. Since this diffracted wave determines the magnitude of the hologram's envelope function, the

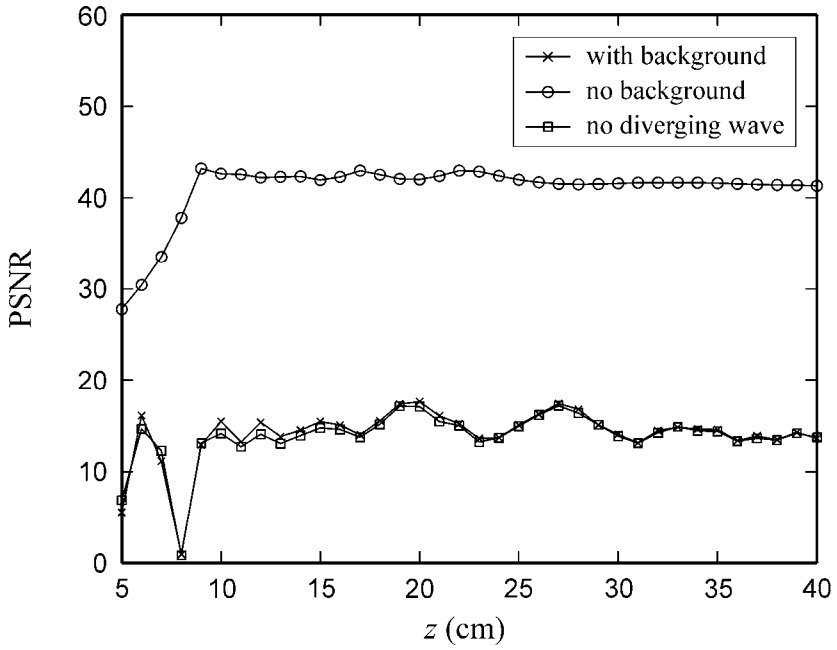

Figure 3.8 PSNR of the image reconstructed from the hologram of a square object with size $2w$ = 125 μm as a function of the recording distance.

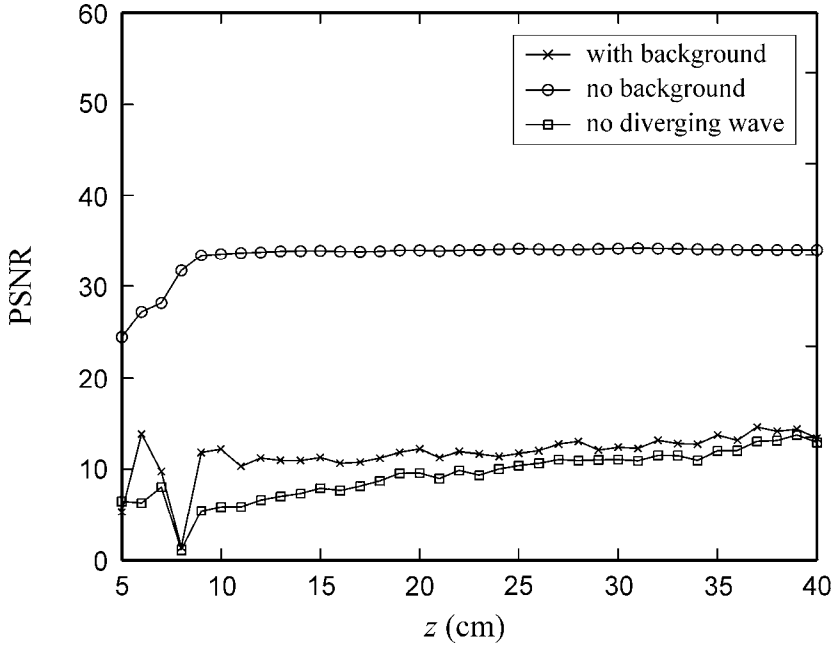

Figure 3.9 PSNR of the image reconstructed from the hologram of a square object with size $2w$ = 250 μm as a function of the recording distance.

amplitude of the diverging wave diffracted by the hologram of the square object is lower than that of the line object. This can be seen from Figs. 3.2(d) and 3.7(d) which show the 1-D cross-sectional intensity of the reconstructed image of the line and the square objects, respectively. Furthermore, the results of the image reconstruction of the square object show a slightly higher PSNR than that of the line object. This may be caused by the fact that the smaller area of the square object results in a smaller distortion of the reconstructed images.

In summary, the above simulation results reveal that the elimination of the coherent background can reduce significantly the out-of-focus virtual image compared to the removal of the diverging wave from the holograms. Since the complex light field of the diverging wave is an unknown factor, the removal of the diverging wave cannot be easily done. As for the background removal method, the amplitude of the uniform background can be simply determined by averaging the intensity of the recorded hologram. Therefore in this thesis, the background removal is employed for solving the twin image problem.

CHAPTER IV

IMAGE RECONSTRUCTIONS FROM IN-LINE HOLOGRAMS OF MULTIPLE OBJECTS

In Chapter III, the quality improvements of the reconstructed image from in-line holograms of single object by removing the background and the diverging wave have been studied through computer simulation. The results show that the background removal can improve the image quality better than the elimination of the diverging wave. In this chapter, the study is focused on the image reconstruction from in-line holograms of multiple objects by using the background removal. Multiple objects distributed in-plane and out-of-plane are considered. As done in the previous chapter, the quality of reconstructed image will be quantitatively measured by means of the PSNR.

4.1 Image reconstructions from in-line holograms of in-plane objects

Let us consider recording of in-line holograms of multiple objects which are geometrically distributed as shown in Fig. 4.1. The separations between object are dz and $d\xi$ in the z and the x directions, respectively. The in-line hologram of multiple line objects are numerically generated by using Eq. (2.2) together with Eqs. (2.12) and (2.14). Figures 4.2(a) and (b) show the in-line hologram of three identical line objects having a diameter 125 μm with and without the coherent background, respectively,

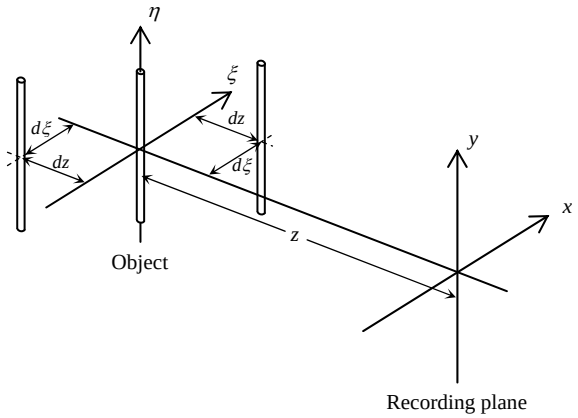

Figure 4.1 Geometrical distribution of multiple line objects separated by *dz* and $d\xi$ along the *z* and the ξ directions, respectively.

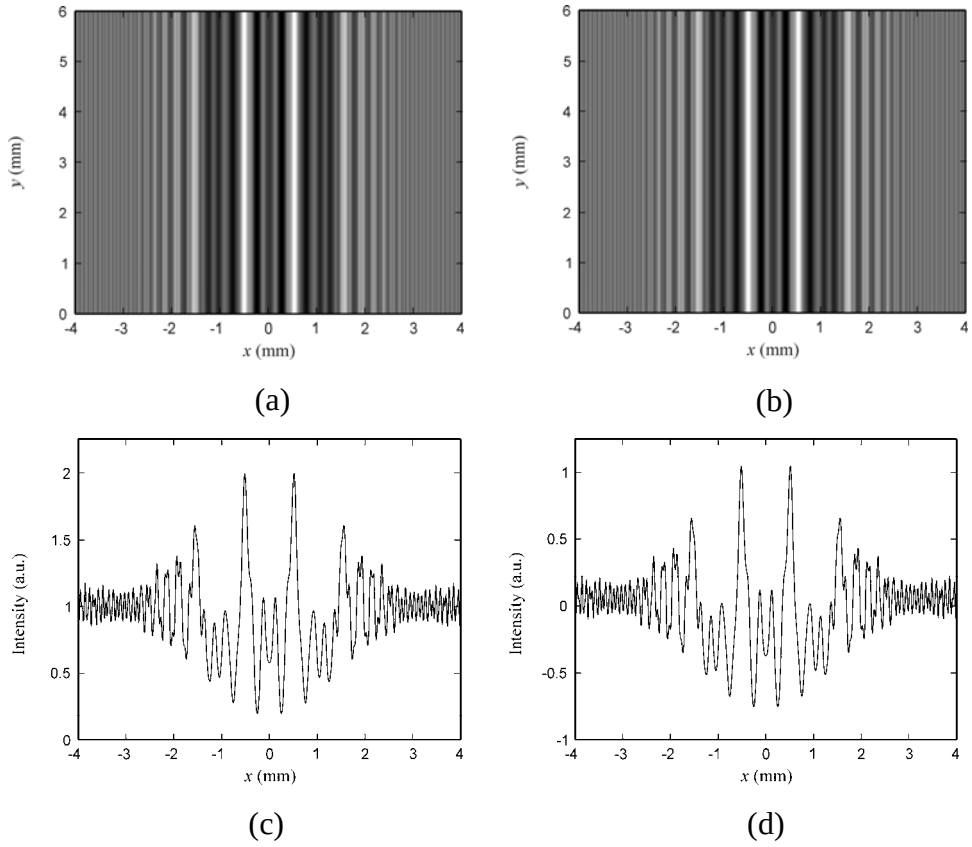

Figure 4.2 In line holograms of three line objects: (a) without modification, and (b) with the background removals. 1-D cross sectional scans of: (c) original hologram, and (d) modified hologram.

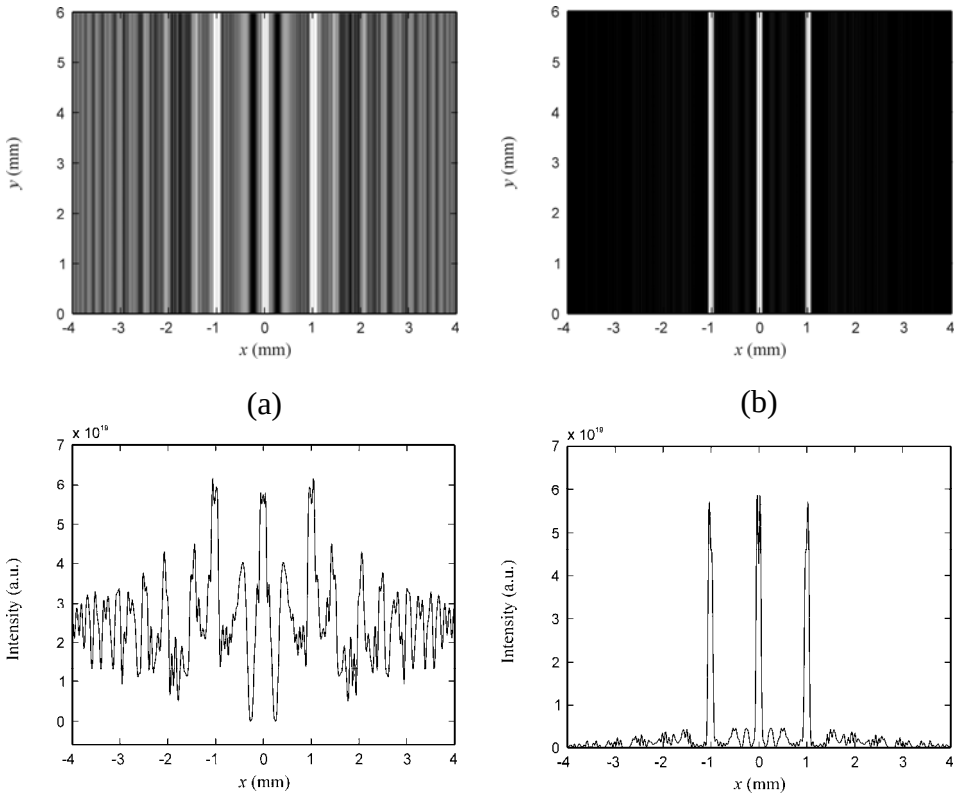

Figure 4.3 Reconstructed images from the holograms of three line objects: (a) without modification, and (b) with the background removals. 1-D cross-sectional scan of the corresponding images: (c) without modification, and (d) with the background removals.

while their corresponding 1-D cross-sectional scans are shown in Figs. 4.2(c) and (d), respectively. All objects are distributed in the same plane at z = 40 cm in front of the recording plane with the separation $d\xi$ equals to 1 mm. Figures 4.3(a) and (b) show the images of the object reconstructed from the corresponding in-line holograms shown in Fig. 4.2, while and their 1-D cross-sectional scans are shown in Figs. 4.3(c) and (d), respectively. In comparison with Fig. 4.3(c) which shows the 1-D intensity

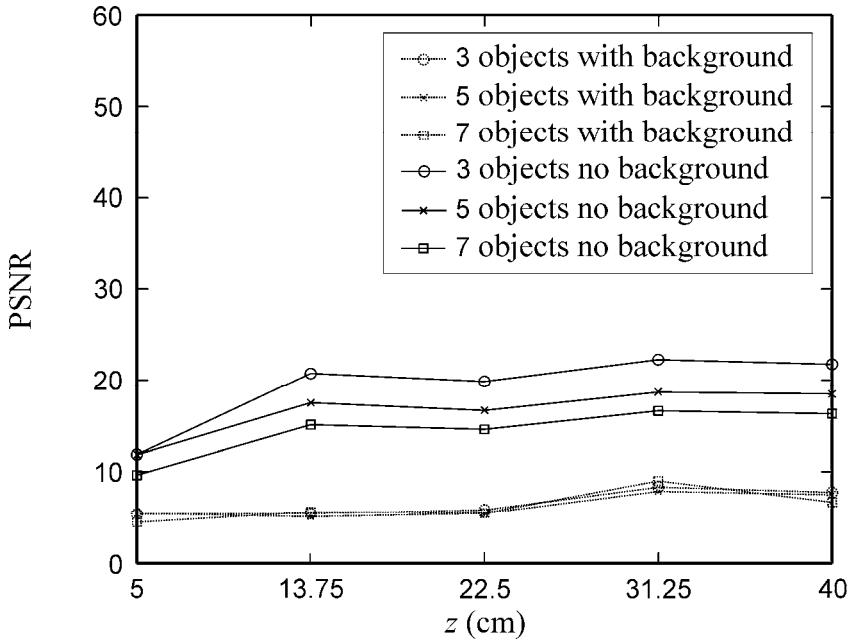

(a)

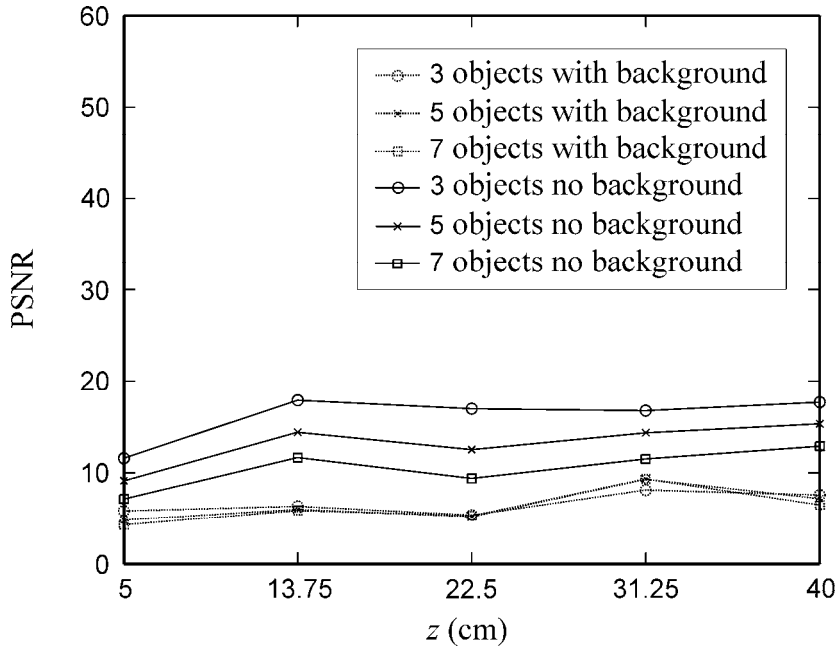

(b)

Figure 4.4 PSNR of images reconstructed from the holograms of multiple line objects having diameter (a) 125 μm and (b) 250 μm with the separation $d\xi = 1$ mm and $dz = 0$ mm.

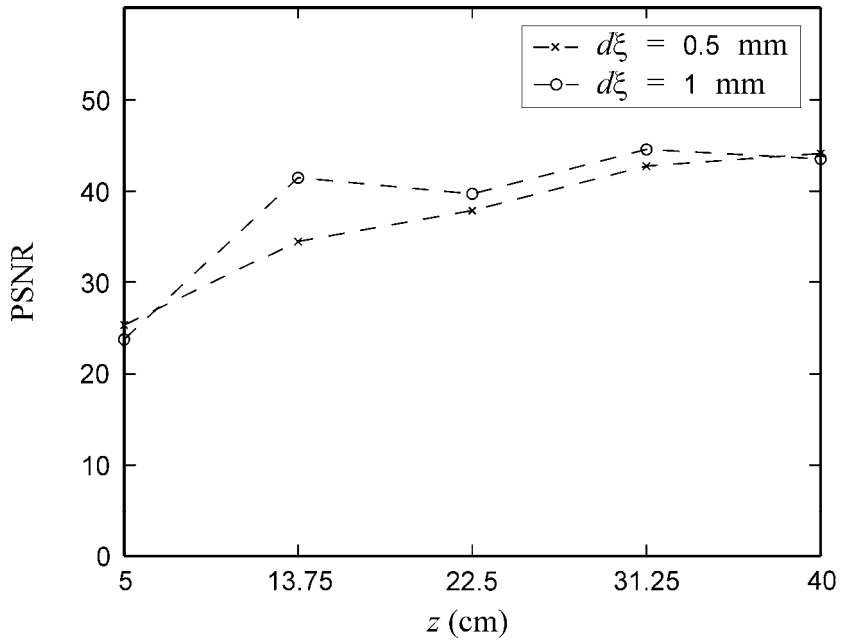

Figure 4.5 PSNR of images reconstructed from the hologram of 3 line objects having diameter 125 μm with the separations $d\xi$ = 0.5 mm and 1 mm as a function of the recording distance.

profile of the image with the contrast reversal reconstructed from the original hologram , the reconstructed image of three line objects can be obviously seen in Fig. 4.3(d). Therefore, the removal of the coherent background improves significantly the quality of the reconstructed image.

Figures 4.4(a) and (b) illustrate the PSNR of the image reconstructed from the holograms of line objects having diameter 125 μm and 250 μm, respectively. The circle, the cross and the square symbols denote the PSNR of 3, 5 and 7 line objects, while the dot and the solid lines represent the results obtained from the holograms without and with the background removals, respectively. The objects are located on the same plane (dz = 0 mm) with their separation $d\xi$ = 1 mm. It can be seen from these two figures that as the number of the objects increases the PSNR reduces,

because more interference patterns overlap. Consequently, the hologram is distorted, producing poorer quality of the reconstructed image. In comparison with Fig. 4.4(a), Fig. 4.4(b) shows that the larger object causes smaller PSNR. This is in agreement with the case of single object.

Figure 4.5 shows the PSNR of images reconstructed from the holograms of 3 line objects having diameter 125 μm with the separation $d\xi$ = 0.5 mm and 1 mm. It can be seen from this figure that the smaller separation yields the lower PSNR. This is due to the fact that the distortion of the hologram of a closely separated object is higher.

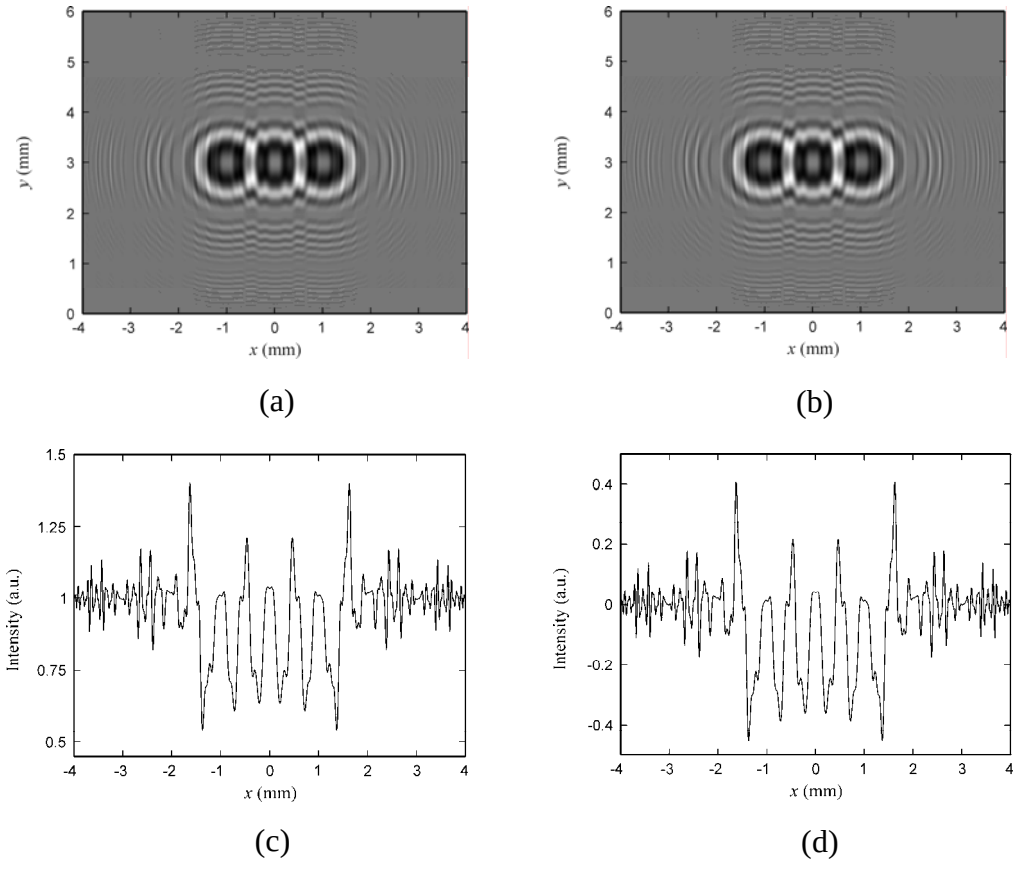

Figure 4.6 In line holograms of three square objects: (a) without modification, and (b) with the background removals. 1-D cross sectional scans of: (c) the original hologram, and (d) modified hologram.

Figures 4.6(a) and (b) show the in-line hologram of three identical square objects having a diameter 250 μm with and without the coherent background, respectively, while their 1-D cross-sectional scans are shown in Figs. 4.6(c) and (d), respectively. They are located on the same plane with z = 40 cm in front of the recording plane with the separations $d\xi$ and $d\eta$ of 1 mm and 0 mm, respectively. Figures 4.7(a) and (b) show the images of the object located at ξ = 0 reconstructed from the corresponding in-line holograms shown in Fig. 4.6, while their 1-D cross-

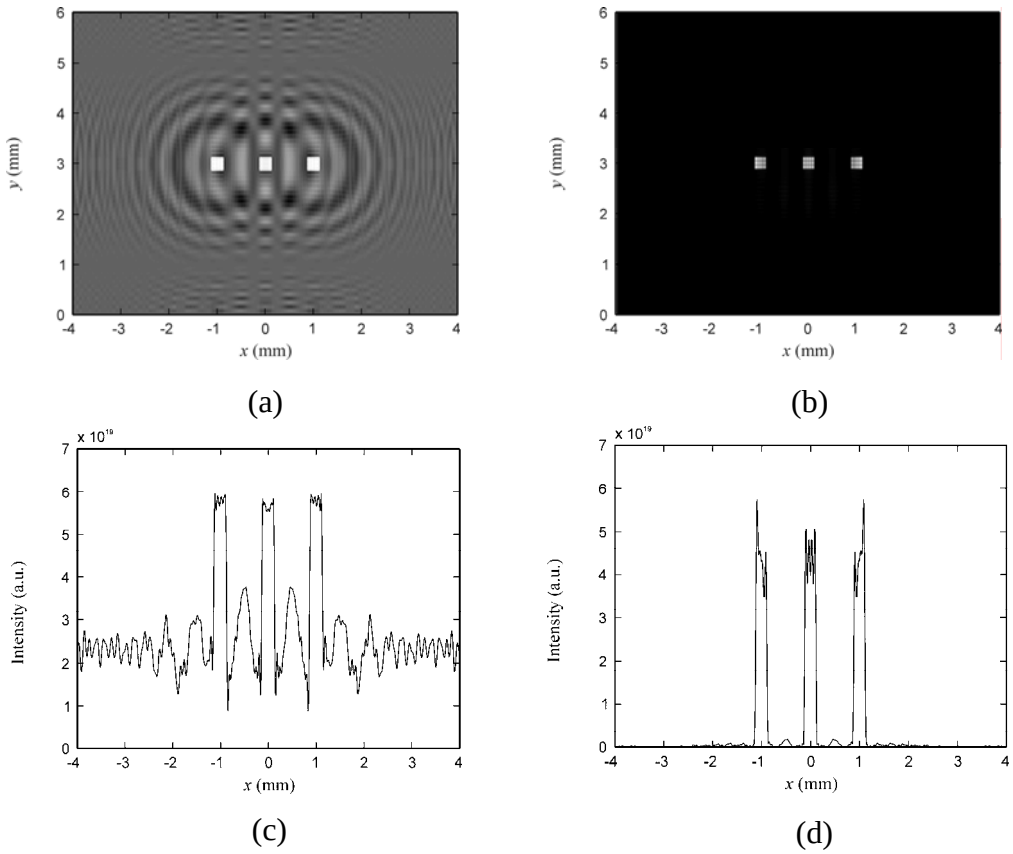

Figure 4.7 Reconstructed images from the holograms of three square objects: (a) without modification, and (b) with the background removals. 1-D cross-sectional scan of the corresponding images: (c) without modification, and (d) with the background removals.

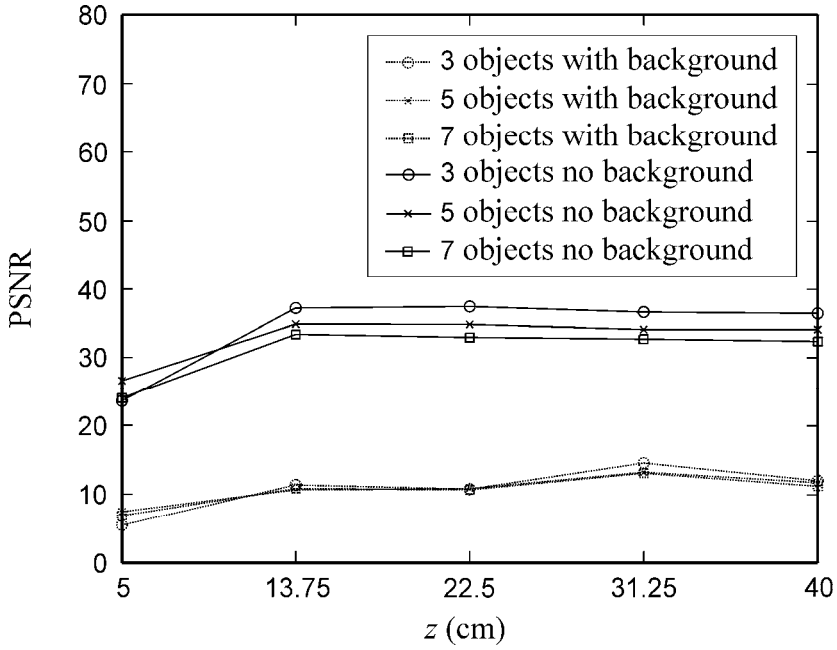

(a)

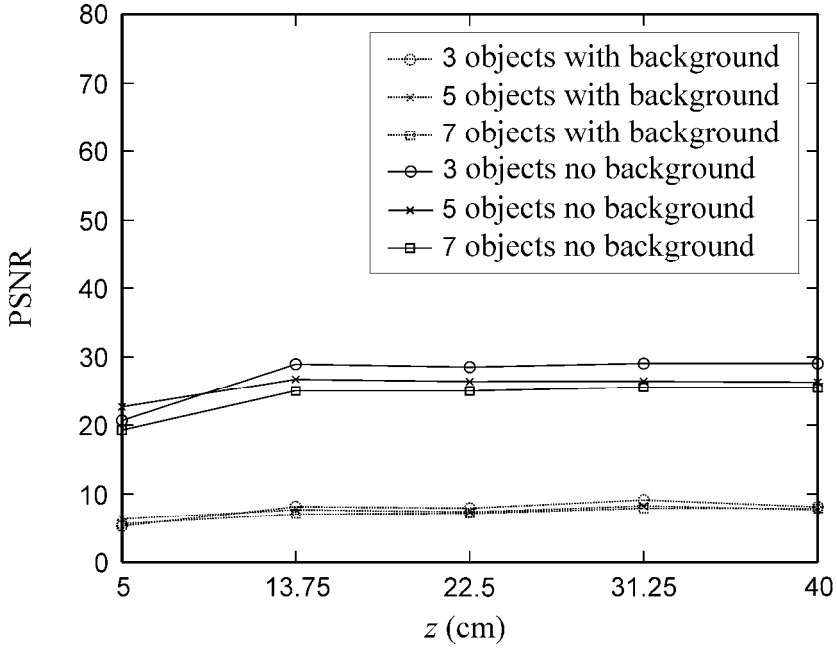

(b)

Figure 4.8 PSNR of images reconstructed from the hologram of multiple square objects having diameter (a) 125 μm and (b) 250 μm with separation $d\xi = 1$ mm and $dz = 0$ mm.

sectional scans are shown in Figs. 4.7(c) and (d), respectively. In Fig. 4.7(c), the image contrast is reversed. It can be clearly seen from Fig. 4.7(d) that the background removal method reduces significantly the out-of-focus virtual image.

The PSNR of the reconstructed image of multiple square objects with w = 62.5 μm and 125 μm are shown in Figs. 4.8(a) and (b), respectively. It can be observed that besides the background removal reduces significantly the out-of-focus virtual image, the similar results as those of the line object are obtained.

From the above results, it can be summarized that the quality of the image reconstructed from the hologram of multiple objects with in-plane distribution depends mainly on the number of the objects, their separation $d\xi$ and the recording distance z. The increase of the number of the objects or the decrease of the horizontal separation degrades the interference pattern of the hologram. This causes the decrease of the quality of the reconstructed image. Since the recording distance determines the frequency of the interference pattern, the PSNR of images reconstructed from the holograms recorded at the longer recording distance is higher than that at the shorter one.

4.2 Image reconstructions from in-line holograms of out-of-plane objects

In this section the image reconstructions from the in-line holograms of the multiple objects that are distributed out-of-plane as shown in Fig. 4.1 are studied. The same line and square objects are used as specimens. The holograms of these multiple objects are also generated from Eq. (2.2). Figures 4.9(a) and (b) show the in-line

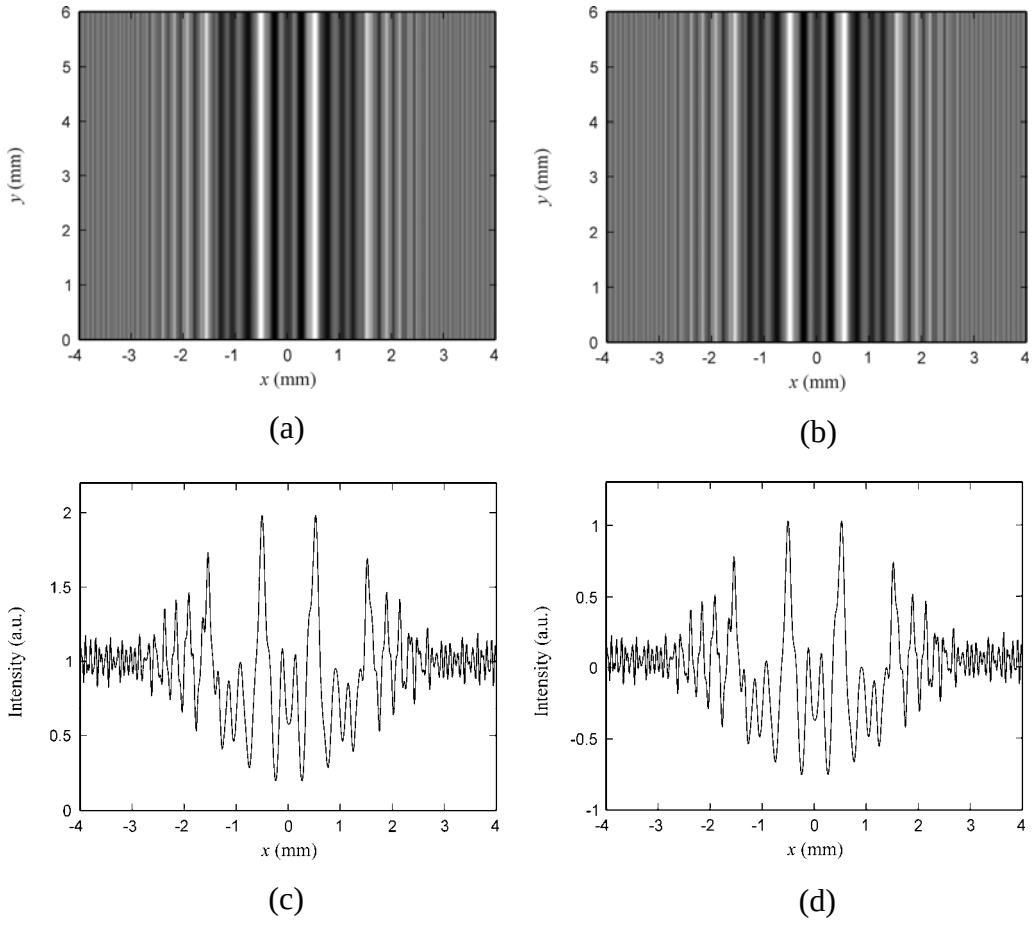

Figure 4.9 In line holograms of three line objects: (a) without modification, and (b) with the background removals. 1-D cross sectional scans of: (c) the original hologram, and (d) the modified hologram.

without the coherent background, respectively, while their 1-D cross-sectional scans are shown in Figs. 4.9(c) and (d). The objects are separated by $d\xi$ = 1 mm and dz = 1 mm. Figures 4.10(a) and (b) show the images of the objects which are reconstructed with respect located at ξ = 0 reconstructed from the corresponding in-line holograms shown in Fig. 4.9, while their 1-D cross-sectional scans are shown in Figs. 4.10(c) and (d), respectively. The recording distance z is 40 cm. Here, Fig. 4.10(c) shows the 1-D intensity profile of the image with the contrast reversal

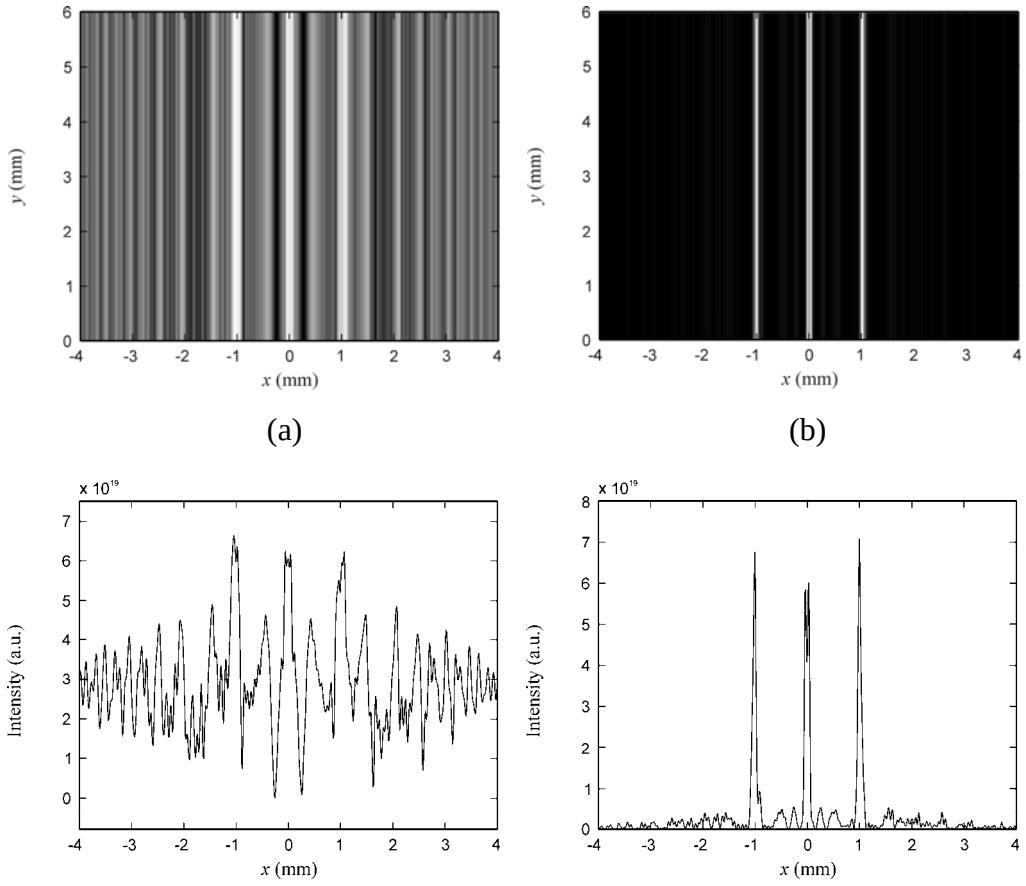

Figure 4.10 Reconstructed images from the hologram of three line objects: (a) without modification, and (b) with the background removals. 1-D cross sectional scans of the corresponding image: (c) without modification, and (d) with the background removals.

reconstructed from the original hologram. In comparison with Fig. 4.10(c), the reconstructed image of three line objects can be obviously seen in Fig. 4.10(d). Figures 4.11(a) and (b) illustrate the PSNR of the image reconstructed from the holograms of line objects having diameter (a) 125 μm and (b) 250 μm, respectively. The circle, the cross and the square symbols denote the PSNR of images of 3, 5 and 7

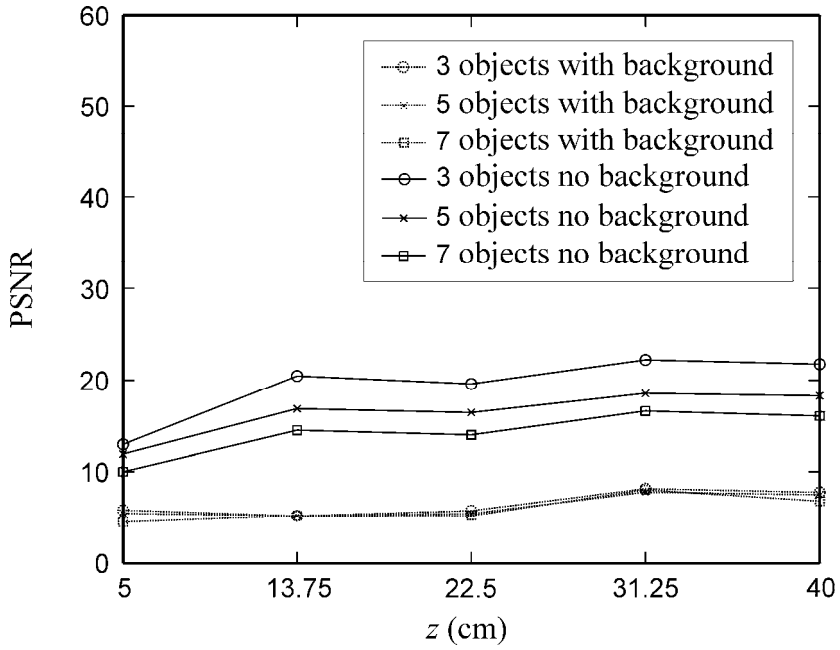

(a)

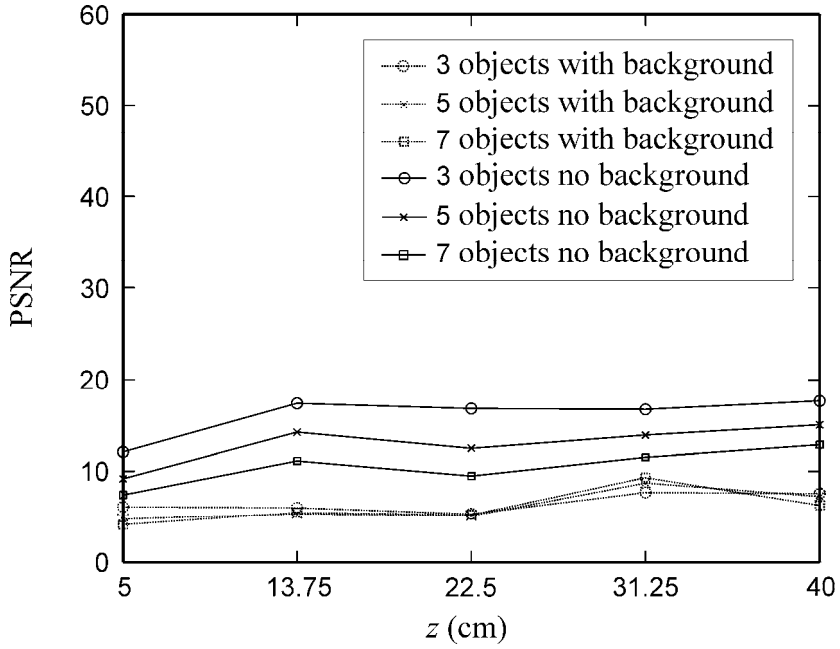

(b)

Figure 4.11 PSNR of image reconstructed from the hologram of multiple line objects having diameter (a) 125 μm and (b) 250 μm with the separation $d\xi = 1$ and $dz = 1$ mm.

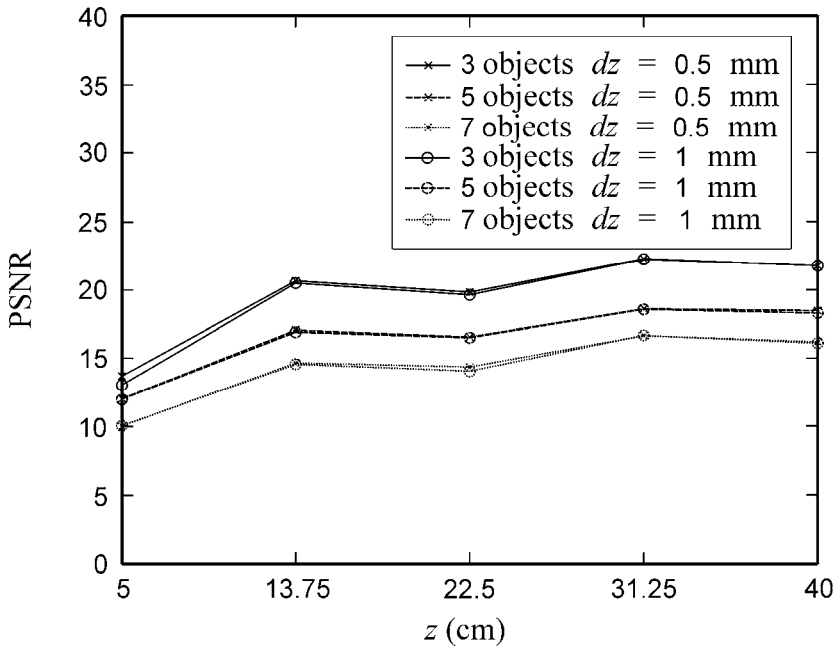

Figure 4.12 PSNR of the image reconstructed from the hologram of multiple line objects having diameter 125 μm with the separation dz = 0.5 mm and 1 mm.

line objects, while the dot and the solid lines represent the results from the holograms without and with the background removals, respectively. In comparison with the reconstruction from the hologram of multiple objects with in-plane distribution depicted in Fig. 4.11, the results have same tendency in that its PSNR is inverse proportional to the number of the object and to the size of the object. However, it is proportional to the recording distance.

Figure 4.12 shows the PSNR of the image reconstructed from the hologram of 3, 5, 7 line objects having diameter 125 μm with the separation $d\xi$ = 1 mm and dz = 0.5 mm and 1 mm. It can be seen from Fig. 4.12 that the separation dz does not affect significantly the quality of the reconstructed image. The image quality depends mainly on the number of objects, their size *w*, the separation $d\xi$ and the recording

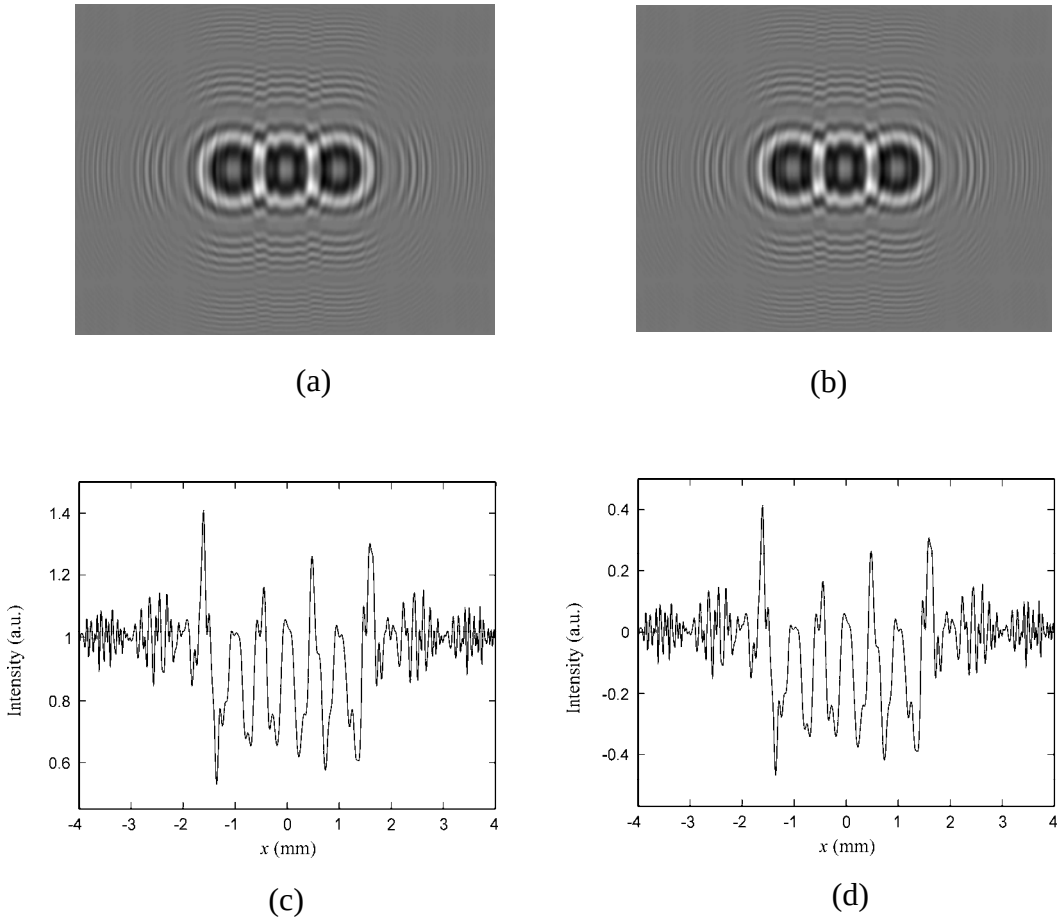

Figure 4.13 In-line holograms of three square objects: (a) without modification, and (b) with the background removals. 1-D cross sectional scans of: (c) the original hologram, and (d) the modified hologram.

distance. The resultant degradation are similar to the case of the multiple objects distributed in the same plane as discussed in the previous section.

Figures 4.13(a) and (b) show the in-line hologram of three identical square objects having w = 125 μm with the separation $d\xi$ = 1 mm and dz = 1 mm. Their corresponding 1-D cross-sectional scans are shown in Figs. 4.13(c) and (d), respectively. Figures 4.14(a), (b), (c) and (d) show the images reconstructed from the corresponding holograms shown in Fig. 4.13. Figure. 4.14(c) shows the 1-D intensity

profile of the image with the contrast reversal reconstructed from the original hologram. The PSNR of the reconstructed image of multiple square objects with w = 62.5 μm and 125 μm are shown in Figs. 4.15(a) and (b), respectively. In comparison with the reconstruction from the holograms of multiple line objects, the similar results are obtained in that the background removal technique reduces

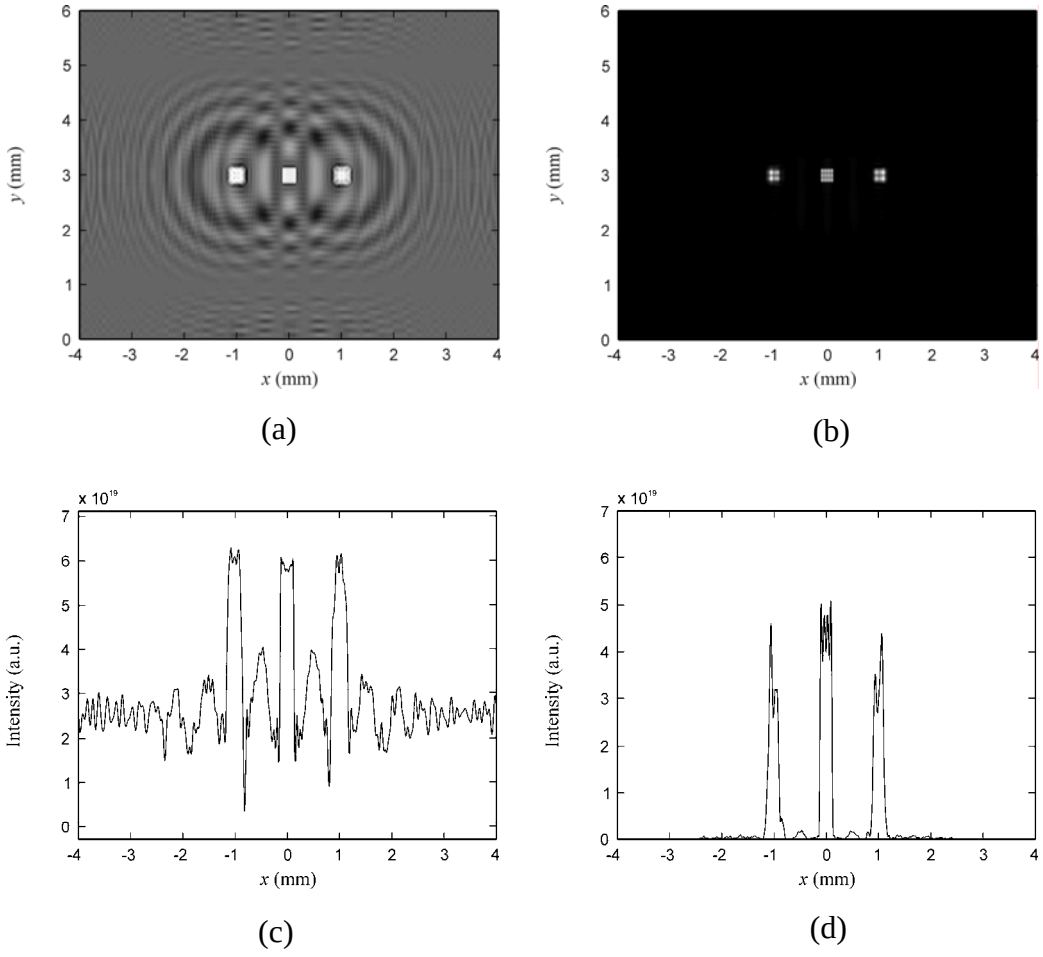

Figure 4.14 Reconstructed images from the holograms of three square objects: (a) without modification, and (b) with the background removals. 1-D cross-sectional scan of the corresponding images: (c) without modification, and (d) with the background removals.

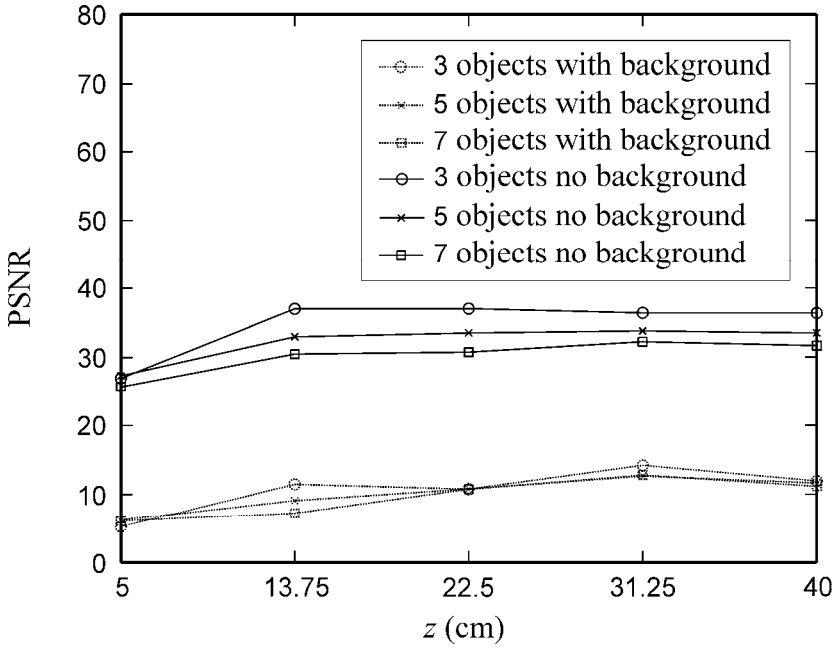

(a)

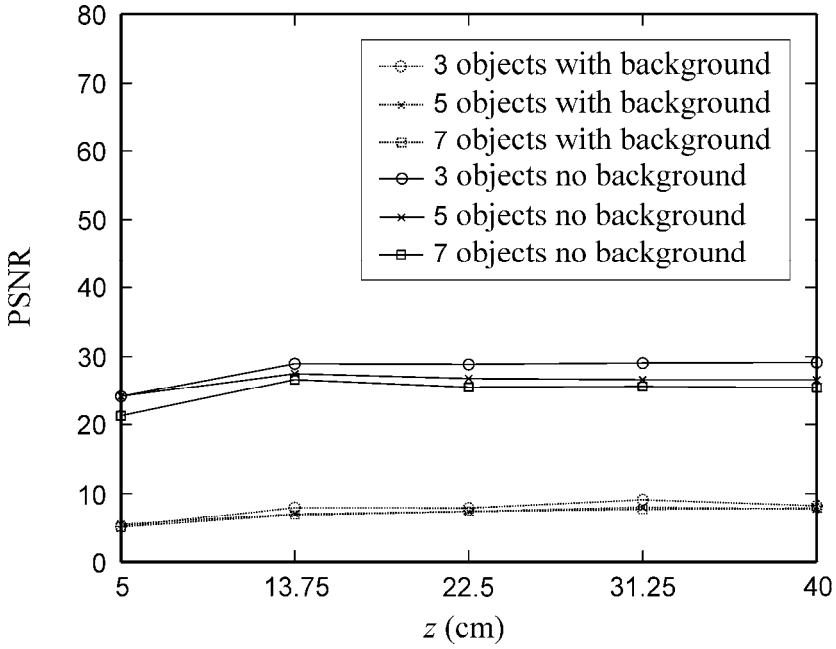

(b)

Figure 4.15 PSNR of image reconstructed from the hologram of multiple square objects having diameter (a) 125 μm and (b) 250 μm with the separation $d\xi = 1$ and $dz = 1$ mm.

significantly the out-of-focus virtual image. It is also found that the separation *dz* of the object along the optical axis does not affect significantly the quality of the reconstructed image of the multiple square objects. However, the image quality is determined by the number of the objects, their size *w*, the separation $d\xi$, and the recording distance.

Equation Chapter 1 Section 1CHAPTER V

CONCLUSIONS

In this thesis, the quality improvement of the reconstructed images by eliminating the coherent background from the in-line holograms is studied by means of computer simulations. The line and the square objects are used the specimens. In the case of the multiple objects, in-plane and out-of-plane object distributions are taken into account. The holograms are numerically generated by calculating the Fresnel diffraction integral. The quality of the reconstructed image is measured by using the PSNR which is computed by comparing the original to the reconstructed images.

Since the out-of-focus virtual image is caused by the directly transmitted wave corresponding to the uniform coherent background and the diverging wave, the reconstructions of images from the in-line holograms of single object by using the removal of these waves are studied in Chapter III. The coherent background is calculated by averaging the total intensities of the hologram. However, since the diverging wave cannot be directly obtained from the hologram, the removal is done by excluding its computation during generating the holograms. The results show that both methods give higher PSNRs than the conventional reconstruction does, however, the remaining coherent background in the image reconstructed from the hologram with the removal of the diverging wave results in a lower PSNR than the removal of the coherent background. This is because the amplitude of the coherent background is greater than the diverging wave. As for the different object size, the larger object

gives lower PSNR. This is because the ringing effect occurs as the consequence of the coherent nature of the hologram and of the amplitude of the diffracted wave which is proportional to the object size. The image reconstructed from the hologram of a square object has a smoother background intensity compared to that of a line object. This may be caused by the fact that the square object has smaller area than the line object does. Consequently, the wave diffracted by the square object which contributes to the background of the reconstructed image has smaller amplitude. Therefore, although the result in this study shows that both removal of the virtual image wave and the coherent background from the holograms can improve significantly the quality of the reconstructed images, the elimination of the coherent background improves the quality of the reconstructed image better than that of the diverging wave. Furthermore, since that the diverging wave is an unknown factor, the removal of this wave from the hologram is hard to be done. In contrast, the removal of the coherent background can be easily accomplished by subtracting the hologram with its averaged intensity, while the higher PSNR can be obtained. Thus, this technique is suitable for improving the reconstructed image from the in-line hologram.

In Chapter IV, the study is extended to the in-line holograms of multiple objects. In this case, only the removal of the coherent background is considered. The results show that the proposed method can still be used for improving the quality of the reconstructed image from these holograms. The increase of the number of the objects as well as the decrease of the object separation $d\xi$ in the object plane reduce the quality of the reconstructed image. This is because the interference pattern of one object overlaps with the others. It is found further that the separation of the object along the optical axis dz does not change significantly the quality of the

reconstructed image. Thus, the quality of the reconstructed image is determined by the object size, the separation between the object in the object plane and the number of the objects.

REFERENCES

REFERENCES

Goodman, J.W. (1996). **Introduction to Fourier optics** (2nd ed.). New York: McGraw-Hill.

Hariharan, P. (1996). **Optical Holography** (2nd ed.). New York: Cambridge University Press.

Kreis T., Adams, M. and Jüptner, W. (1999). Digital in-line holography in particle measurement. **Proceedings SPIE.** 3744: 54-64.

Leith, E.N. and Upatnieks, J. (1962). Reconstructed wavefronts and communication theory. **Journal of the Optical Society of America.** 52: 1123-1130.

Liu, G. and Scott, P.D. (1987). Phase retrieval and twin-image elimination for in-line Fresnel holograms. **Journal of the Optical Society of America A.** 4: 159-165.

Pan, G. and Meng, H. (2003). Digital holography of particle fields : reconstruction by use of complex amplitude. **Applied Optics.** 42: 827-833.

Pitlak, R.T., Page, R. and Selvin, N.P. (1976). Limitation of transmission holography in particle analysis. **Holosphere.** 5: 1-4.

Soontaranon, S., Widjaja, J. and Asakura, T. (2002). Direct analysis of in-line particle holograms by using wavelet transform and envelope reconstruction method. **Optik.** 113(11): 489-494.

Soontaranon, S., Widjaja, J. and Asakura, T. (2004). Improved holographic particle sizing by using absolute value of the wavelet transform. **Optics Communications.** 240: 253-260.

Thomson, B.J. (1963). Fraunhofer diffraction pattern of opaque objects with coherent background. **Journal of the Optical Society of America.** 53: 1350.

Tyler, G.A. and Thomson, B.J. (1976). Fraunhofer holography applied to particle size analysis. **Optica Acta.** 23: 685-700.

Yang, S., Zhang X. and Mitra, S. (1999). Performance of lossy compression algorithms from statistical and perceptual metrics. **Proceedings 12th IEEE Symposium**: 199-204.

Zhang, Y., Pedrini G., Osten, W. and Tiziani, H.J. (2003). Whole optical wave field reconstruction from double or multi in-line holograms by phase retrieval algorithm. **Optics Express.** 11: 3234-3240.

CURRICULUM VITAE

FIRST NAME: Phacharawadee

LAST NAME: Raweng

GENDER: Female

NATIONALITY: Thai

DATE OF BIRTH: May 18, 1980

EDUCATION BACKGROUND:

- Bachelor of Engineering in Telecommunication Engineering

  May 24, 1998 – April 10, 2003

  Suranaree University of Technology, Thailand.